Review of ultrasound image guidance in external beam radiotherapy part II: intra-fraction motion management and novel applications

2016 Phys. Med. Biol. 61 R90

(http://iopscience.iop.org/0031-9155/61/8/R90)

OPEN ACCESS
IOP Publishing | Institute of Physics and Engineering in Medicine Physics in Medicine & Biology
Phys. Med. Biol. **61** (2016) R90–R137 doi:10.1088/0031-9155/61/8/R90

Topical Review

Review of ultrasound image guidance in external beam radiotherapy part II: intra-fraction motion management and novel applications

Tuathan O'Shea[1], Jeffrey Bamber[1], Davide Fontanarosa[2,3], Skadi van der Meer[2], Frank Verhaegen[2,4] and Emma Harris[1]

[1] Joint Department of Physics, Institute of Cancer Research and Royal Marsden NHS Foundation Trust, Sutton, London SM2 5NG, UK
[2] Department of Radiation Oncology (MAASTRO), GROW School for Oncology and Developmental Biology, Maastricht University Medical Center (MUMC), Maastricht 6201 BN, The Netherlands
[3] Oncology Solutions Department, Philips Research, High Tech Campus 34, Eindhoven 5656 AE, The Netherlands
[4] Medical Physics Unit, Department of Oncology, McGill University, Montréal, Québec, Canada

E-mail: emma.harris@icr.ac.uk

Received 3 June 2015, revised 16 November 2015
Accepted for publication 19 January 2016
Published 22 March 2016

Abstract

Imaging has become an essential tool in modern radiotherapy (RT), being used to plan dose delivery prior to treatment and verify target position before and during treatment. Ultrasound (US) imaging is cost-effective in providing excellent contrast at high resolution for depicting soft tissue targets apart from those shielded by the lungs or cranium. As a result, it is increasingly used in RT setup verification for the measurement of inter-fraction motion, the subject of Part I of this review (Fontanarosa *et al* 2015 *Phys. Med. Biol.* **60** R77–114). The combination of rapid imaging and zero ionising radiation dose makes US highly suitable for estimating intra-fraction motion. The current paper (Part II of the review) covers this topic. The basic technology for US motion estimation, and its current clinical application to the prostate, is described here, along with recent developments in robust motion-estimation algorithms, and three dimensional (3D) imaging. Together, these are likely to drive an increase in the number of future clinical studies and the range of cancer sites in which

US motion management is applied. Also reviewed are selections of existing and proposed novel applications of US imaging to RT. These are driven by exciting developments in structural, functional and molecular US imaging and analytical techniques such as backscatter tissue analysis, elastography, photoacoustography, contrast-specific imaging, dynamic contrast analysis, microvascular and super-resolution imaging, and targeted microbubbles. Such techniques show promise for predicting and measuring the outcome of RT, quantifying normal tissue toxicity, improving tumour definition and defining a biological target volume that describes radiation sensitive regions of the tumour. US offers easy, low cost and efficient integration of these techniques into the RT workflow. US contrast technology also has potential to be used actively to assist RT by manipulating the tumour cell environment and by improving the delivery of radiosensitising agents. Finally, US imaging offers various ways to measure dose in 3D. If technical problems can be overcome, these hold potential for wide-dissemination of cost-effective pre-treatment dose verification and *in vivo* dose monitoring methods. It is concluded that US imaging could eventually contribute to all aspects of the RT workflow.

Keywords: tracking, ultrasound, guidance, radiotherapy, elastography, photoacoustics, dosimetry

(Some figures may appear in colour only in the online journal)

List of abbreviations

ABC	Active breathing control
AP	Anterior–posterior
ARFI	Acoustic radiation force impulse (imaging)
BTV	Biological target volume
CDUS	Colour Doppler ultrasound
CEUS	Contrast enhanced ultrasound
CPD	Colour pixel density
CT	Computed tomography
DCE-US	Dynamic contrast enhanced ultrasound
DIL	Dominant intra-prostatic lesion
DSC	Dice similarity coefficient
EM	Electromagnetic
FDG-PET	Fluorodeoxyglucose positron emission tomography
FOV	Field of view
FPS	Frames per second
GV	Gas nanovesicle
IGRT	Image guided radiotherapy
IMRT	Intensity modulated radiotherapy
kV	Kilovolt
LED	Light emitting diode
linac	Linear accelerator
LR	Left right
MAGIC	Methacrylic and ascorbic acid in gelatine initiated by copper
MBF	Mid band fit

MIP	Maximum intensity projection
MLC	Multi-leaf collimator
mMRI	Multi-parameter magnetic resonance imaging
MR	Magnetic resonance
MRI	Magnetic resonance imaging
MV	Megavoltage
MVD	Microvessel density
NCC	Normalised cross-correlation
NIST	National Institute of Standards and Technology
OCT	Optical computed tomography
PAG	Polyacrylamide gel
PDUS	Power doppler ultrasound
PET	Positron emission tomography
pO_2	Oxygen partial pressure
PTV	Planning target volume
RF	Radio frequency/radio-frequency
ROC	Receiver operating characteristic
ROI	Region of interest
RPV	Reference planning volume
RT	Radiotherapy/radiation therapy
RTOG	Radiation therapy oncology group
SAD	Sum of absolute differences
SBRT	Stereotactic body radiation therapy
SE	Strain elastography
SD	Standard deviation
SI	Spectral intercept/superior inferior
SNR	Signal to noise ratio
SS	Spectral slope
SSD	Sum of squared differences
SWE	Shear wave elastography
SOS	Speed of sound
TE	Transient elastography
THPC	Tetrakis (hydroxymethyl) phosphonium chloride
TPUS	Transperineal ultrasound
UBCs	Ultrasound backscatter characteristics
US	Ultrasound
USMI	Ultrasonic molecular imaging
UIB	Ultrasound integrated backscatter
VEGFR-2	Vascular endothelial growth factor receptor type 2
VMAT	Volumetric modulated arc therapy
1D	One dimensional
2D	Two dimensional
3D	Three dimensional
4D	Four dimensional

1. Introduction

Within the topic of image guided radiotherapy (IGRT) research there is a growing interest in ultrasound (US) imaging, which offers rapidly developing technology for real-time

two-dimensional (2D) and three-dimensional (3D) anatomical and functional inter-fraction and intra-fraction imaging at high frame and volume rates. Earlier review papers have dealt with US-based anatomical localization (Kuban *et al* 2005) or 3D US technology (Fenster *et al* 2001). The current review and its companion paper (Fontanarosa *et al* 2015) are the first to cover extensively the recent progress and growing applications of modern US imaging in radiotherapy (RT). Part I (Fontanarosa *et al* 2015) focused on the use of US for inter-fraction motion correction. Here, in Part II, we address the potential benefits of further integration of US imaging into the RT workflow, including: intra-fraction motion correction, biological target volume (BTV) identification, prediction and monitoring of tumour response, normal tissue toxicity assessment, therapeutic effect enhancement, and dosimetry. Figure 1 provides a guide to the potential applications of US to specific stages of the RT workflow, and where in this review these topics are discussed. This review does not consider the use of US to detect tumour recurrence post-RT, as this is covered in reviews on the use of US for cancer diagnosis.

2. US based intra-fraction motion management

2.1. Intra-fraction motion

Intra-fraction translation, rotation or deformation of the target (tumour) during radiation beam delivery has a negative impact on RT which is well understood (Yorke *et al* 2008). A study by Langen and Jones (2001) reviewed organ motion relevance to RT. Motion statistics, for US-accessible treatment sites are given in table 1. For treatment sites influenced most by respiratory motion, such as the liver, this motion can significantly reduce accuracy of delivery (Von Siebenthal *et al* 2007). Simulated gating and dynamic multi-leaf collimator (MLC) tracking have been shown to improve dose distributions for prostate (Colvill *et al* 2014), which can experience significant (non-respiratory based) motion in some treatment fractions (Noel *et al* 2009, Ng *et al* 2012).

The various methods that can measure intra-fraction motion, whilst a patient is treated on a standard C-arm linac, can be divided into techniques that use (1) external surface motion, (2) implanted markers (electromagnetic or metallic), (3) US or (4) x-ray imaging (see figure 2). For an overview of the different IGRT techniques the reader is referred to Jaffray (2012) and De Los Santos *et al* (2013). Table 2 summarises the key features of current and emerging intra-fraction motion estimation technologies for controlling RT beams by tracking or gating, and the potential advantages and disadvantages of each. Advantages that US holds over other techniques include the combination of high accuracy, high spatial resolution, high temporal resolution, ability to account for tissue deformation by direct monitoring of internal tissue motion, and no ionising radiation dose or invasion. Disadvantages include inaccessibility of US to tissues shielded by air or bone, potential for the US transducer to interfere with the RT dose distribution, and, for some 3D US technologies, restriction on imaging volume rate. These latter two practical issues will be discussed below in section 3.3. The emergence of megavoltage (MV) treatment machines which combine magnetic resonance (MR) image-guidance share many of the advantages of US but their use (like US) has yet to be fully explored (Kirkby *et al* 2008, Raaijmakers *et al* 2008).

2.2. Implementation of US intra-fraction motion management

Relative to x-ray based techniques, the use of US for intra-fraction motion management is at an early stage (see table 2). The following section is intended to familiarise the reader with the methods used to estimate tissue motion using US.

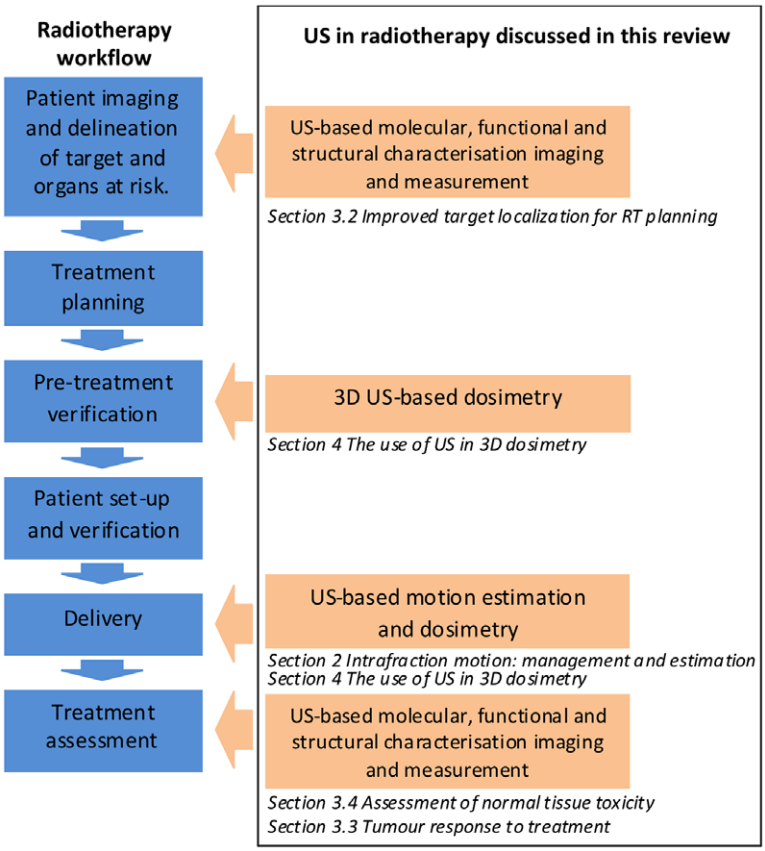

Figure 1. The potential applications of US in the radiation treatment chain and the sections of this review where these applications are discussed. The use of US imaging for patient set-up and verification was discussed in Part I of this review (Fontanarosa *et al* 2015).

2.2.1. US motion estimation techniques. There are two types of US motion estimation techniques: direct and indirect. Direct methods detect echo motion, whether it corresponds to homogeneous speckle or resolved tissue structure, such as anatomical features. Indirect methods estimate the motion of segmented boundaries (see figure 3).

Direct (echo-based) methods: Motion can be estimated without region or boundary segmentation, using (i) US echo fluctuation or (ii) tracking methods, either of which may use the phase or the magnitude of the US echo signal (Eckersley and Bamber 2004). Fluctuation (e.g. Doppler) methods have not been applied to motion estimation in RT and will not be discussed further. Tracking methods, also known as time-domain methods (Hein and O'brien 1993, Eckersley and Bamber 2004), measure displacement as the shift in location needed to re-establish echo correlation (Eckersley and Bamber 2004) and have been used to estimate tissue and phantom motion in RT.

US images possess a grainy structure called speckle (Burckhardt 1978). Speckle is an image pattern that is unique to a region of tissue, and is created by the interference between echoes from US scatterers that are too close to each other to be separately resolved (Bamber 1993, Chen *et al* 1995). It provides image structure that accurately follows tissue motion, even when no

Table 1. Motion statistics for various organs accessible by US. These motion data were acquired with a variety of imaging modalities including x-ray imaging, magnetic resonance imaging (MRI), 4DCT and US.

Tissue	Motion statistic	Displacement (mm) or percentage (%)	Observer
Breast (cavity)	Range (3D)	0.8–3.8	Glide-Hurst *et al* (2015)
Breast (ipsilateral)	Range (3D)	0.7–3.0	Glide-Hurst *et al* (2015)
Liver	Mean (range)	17.6 (5.6–39.5)	Worm *et al* (2013)
	Mean ± S.D.	24.4 ± 16.4	Bussels *et al* (2003)
	Mean ± S.D.	13.0 ± 5.0	Weiss *et al* (1972)
	Mean	14	Harauz and Bronskill (1979)
	Mean (range)	25 (10–40)	Suramo *et al* (1983)
	Mean (range)	10 (5–17)	Davies *et al* (1994)
Kidney	Mean (range)	19 (10–40)	Suramo *et al* (1983)
	Mean (range)	11 (5–16)	Davies *et al* (1994)
	Mean ± S.D.	16.9 ± 7.9	Bussels *et al* (2003)
	Mean	<10	Pham *et al* (2014)[a]
Pancreas	Mean (range)	20 (10–30)	Suramo *et al* (1983)
	Mean (range)	20 (0–35)	Bryan *et al* (1984)
	Mean ± S.D.	23.7 ± 15.9	Bussels *et al* (2003)
Prostate (supine)	Range (AP)	−4.6–6.8	Huang *et al* (2002)
	Mean ± S.D.	0.6 ± 0.4	Butler *et al* (2013)
	Margins (LR, AP, IS)[b]	1.8, 5.8, 7.1	Litzenberg *et al* (2006)
	Mean time > 3, 5 mm	14%, 3%	Langen *et al* (2008)
	Time > 3, 5, 7, 10 mm	5.6%, 2.2%, 0.7%, 0.4%	Ng *et al* (2012)
Prostate (prone)	Mean ± S.D.	1.2 ± 0.6	Butler *et al* (2013)
Cervix	Margins (fundus, os)[c]	10, 4.5	Chan *et al* (2008)
	Maximum	10.6	Kerkhof *et al* (2009)
	Mean ± S.D. (AP)	2.9 ± 2.7	Haripotepornkul *et al* (2011)
Uterus	Mean ± S.D. (AP)	7.0 ± 9.0	Taylor and Powell (2008)
Bladder	Maximum	58	McBain *et al* (2009b)
	Volume increase	101%	McBain *et al* (2009a)
	S.D.	5	Meijer *et al* (2003)
	Maximum	15	Foroudi *et al* (2013)
Rectum	Maximum	30	Muren *et al* (2004)
	Margin (systematic, random)[d]	6, 16	Muren *et al* (2004)

[a] Review paper—mean of 15 publications (free breathing).
[b] Planning target volume (PTV) margin.
[c] Internal target volume margin.
[d] Planning organ at risk volume (PRV) margin.

resolved tissue structure is present, so long as the tissue stays in view without excessive deformation or rotation and no changes occur to the US imaging parameters (e.g. US beam direction, frequency, pulse shape or beam shape). Violation of these conditions results in a speckle pattern that changes, or decorrelates, as it moves. When resolved tissue structure is present, its motion may be followed directly, although similar conditions apply as for speckle tracking. Direct methods tend to be based on the application of similarity measures to estimating the motion of regions of US speckle or localised resolved tissue structure (Harris *et al* 2010); commonly it is a combination of both (figure 3). We therefore refer to all such methods as echo pattern matching.

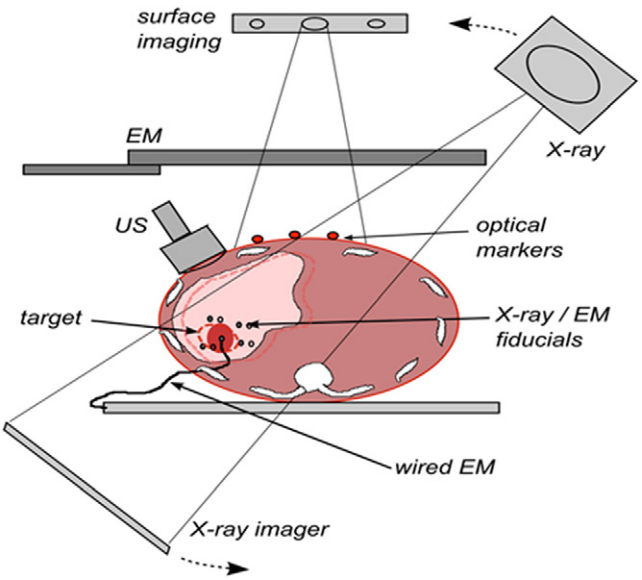

Figure 2. Methods of intra-fraction motion estimation: optical surface imaging, kV x-ray, wired and wireless (induction-based) EM fiducials and US imaging.

Echo pattern matching is illustrated in figure 4 for a sector scan. A region of interest (ROI), containing a unique echo pattern, is defined in an US image (acquisition 1). In a subsequent US image (acquisition 2), a pattern matching algorithm searches for the region that best matches the echo pattern in the ROI, identified using a similarity measure such as the normalised cross correlation coefficient (NCC) (e.g. Bonnefous and Pesque 1986), sum of absolute differences (SAD) (e.g. Bohs *et al* 1993), or sum of squared differences (SSD) (Langeland *et al* 2003).

Indirect (image segmentation-based) methods: Indirect motion estimation methods involve image analysis methods to segment an element of anatomy, e.g. the prostate boundary. Once segmentation has been achieved in each acquisition, a positional measure such as centre-of-mass of the object (or objects) detected may be extracted to provide, over many acquisitions, a time-varying displacement. Such segmentation may, however, not always be possible using US data alone due to a lack of reliable landmarks (Yang and Fei 2012).

Segmentation of a clearly defined object displayed with high echo image contrast (e.g. a fluid filled cavity) can be relatively straightforward (Sarty *et al* 1998). However, US images of a target such as the prostate are difficult to segment because of relatively low contrast and artefacts such as those due to shadowing, meaning that image processing operators such as edge detectors are inadequate by themselves. More complex methods such as the active contouring (Kass *et al* 1988) have been developed but require initialisation by user defined curves (Pathak *et al* 1998). Fully automated 3D segmentation based on atlas registration and texture priors has shown promise when compared with manual segmentation in prostate transrectal US (Yang and Fei 2012). For intra-fraction motion, segmentation would have to be both rapid and fully automated. Fast segmentation has been investigated for image guidance of surgery of the kidney (Ahmad *et al* 2006) and liver (Angelini *et al* 2005, Foroughi *et al* 2006), radiosurgery of the liver (Lee *et al* 2011) and for ventricular volume estimation in echo-cardiography (Angelini *et al* 2005, Hansegård *et al* 2007).

The choice of whether to employ a direct or indirect algorithm (or a combination of both) may depend on the availability and quality of features for reliable segmentation. Direct

Table 2. A comparison of (first use) commercial and research intra-fraction motion estimation methods and technologies. Technologies are grouped by method. Cancer sites for which technology accuracy was evaluated are given in column 4. Some potential advantages and disadvantages of each method are listed in columns 7 and 8.

Method	Motion estimation technology	Publication(s)	Evaluation site	Accuracy	Temporal resolution	Advantages	Disadvantages
EM	Varian Calypso®	Balter *et al* (2005)	Phantom	0.54 mm	0.1 s	No dose, high sample rate	Invasive, height restriction, non-compliant with composite materials, not compatible with MRI
		Kupelian *et al* (2007)	Prostate	1.9 mm			
EM	Micropos RAYPILOT®	Kindblom *et al* (2009)	Prostate	1.7 ± 1.0 mm		No dose, High sample rate	Invasive (catheter insertion)
		Ravkilde *et al* (2011)	Lung	0.98 mm			
Near-IR	VisionRT GateRT®	Hughes *et al* (2009)	Lung (gating)	Good correlation (>0.8) with spirometry	0.05 s	No dose,high sample rate, non-invasive	Assumes correlation with internal motion
IR	Microsoft Kinect™	Xia and Siochi (2012) Alnowami *et al* (2012)	Respiratory (surface)	High correlation (>0.96) with strain gauge, <1 mm, 1 mm/1°	0.03 s	No dose, low cost	Assumes correlation with internal motion
	(Research)	Aoki *et al* (2012)					
X-ray/IR	Accuray synchrony™	Hoogeman *et al* (2009) Ozhasoglu *et al* (2008)	Lung	<2.5 mm	0.04−0.025 s (CCD cameras) 60–120 s (x-ray imaging)	High sample rate, no dose	Migration, assumes correlation with internal motion
X-ray/IR	Novalis ExacTrac®	Chang *et al* (2011) Udrescu *et al* (2013)	Lung (gating)	1.9 mm	0.07 s	High sample rate	Radiation dose (less than kV CBCT), invasive (implantation), increased treatment time
		Ackerly *et al* (2011)	Intracranial	1.35 mm			
X-ray	Accuray fiducial tracking	Fu and Kuduvalli (2008)	Head and Neck phantom	0.33 ± 0.16 (max: 0.86 mm) at 0 mm from imaging centre	30–60 s (typical), 5 s (minimum)	High accuracy displacement/ rotation tracking	Radiation dose (Prostate: 196 images, 16 mSv), Invasive, Limited sample rate
X-ray	KIM (Research)	Ng *et al* (2012)	Prostate	0.46 mm	0.1 to 0.2 s	Image plus 3 segmented fiducials	Radiation dose (61 mSv at 10 Hz), Invasive

(*Continued*)

Table 2. (*Continued*)

Method	Motion estimation technology	Publication(s)	Evaluation site	Accuracy	Temporal resolution	Advantages	Disadvantages
X-ray	Fluoroscopy	Adamson and Wu (2008, 2010)	Prostate	0.30–0.68 mm (SD)	0.03 s	High imaging rate	Radiation dose, Invasive (fiducials)
	(Research)	Shirato *et al* (2000)	Lung (gating)	1.5 mm			
		Kitamura *et al* (2003)	Liver				
		Kinoshita *et al* (2008)	Breast				
X-ray	MV/EPID (Research)	Keall *et al* (2004)	Phantom (respiratory)		0.1 s	Standard on Linac, high sample rate	Radiation dose, Poor image quality
Ir-192 implant	Navotek RealEye™ motion	Shchory *et al* (2009)	Prostate (canine)	1.1 ± 0.4 mm	—	—	Invasive, one point, no rotational information
		Shchory *et al* (2010)		0.89 mm			
		Schifter *et al* (2008)	Phantom	0.3 mm			
		Neustadter *et al* (2010)					Radiation dose (patient: 64 mSv, spouse: 0.25 mSv, radiographer: 0.34 mSv)
US	Elekta clarity autoscan	Lachaine and Falco (2013)	Prostate phantom	0.2–0.4 mm (SD)	2.5 s	3D soft-tissue information, no dose, non-invasive (no fiducials)	Unfamiliar technology in RT, need for probe position optimisation (for other sites)
MR (0.35 T)	Viewray™	Noel *et al* (2012)	Bowel	Visually assessed	0.25 s	No dose, high sample rate, non-invasive	Cobalt-60, low strength magnetic field

Key: EM, electromagnetic; IR, infrared; US, ultrasound; MR, magnetic resonance.

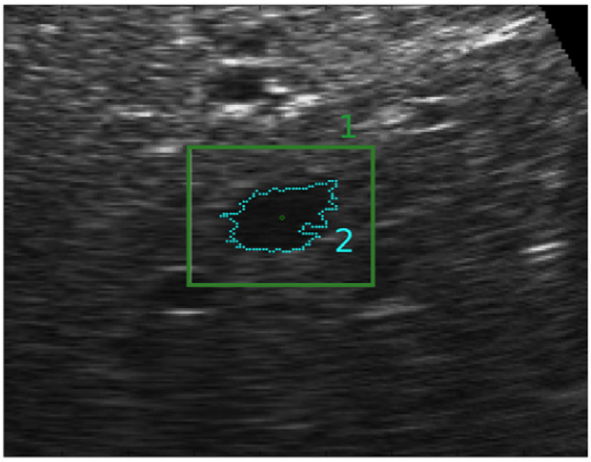

Figure 3. Motion in US image sequences can be estimated by (1) measuring echo motion directly, e.g. echo pattern matching which does not distinguish between homogeneous (speckle) regions and anatomical features (green box) or (2) indirect methods which estimate the motion of segmented boundaries (light blue dotted-line).

methods are the most commonly studied and the only ones used to date in a commercial US guided RT system (Lachaine and Falco 2013). A number of interesting direct approaches to motion estimation in long 2D B-mode *in vivo* US liver sequences were recently presented (De Luca *et al* 2015).

2.2.2. Factors influencing the accuracy of direct echo-based motion estimation. When implementing a direct echo-based technique it is important to consider a number of factors which can influence the accuracy of the motion estimation (some of these factors are also relevant to indirect (segmentation-based) approaches). Motion estimation accuracy can be affected by factors specific to the tissue (target) of interest, such as depth, speed and type of motion. Others factors are specific to the imaging, data type and algorithmic parameter choices. A full discussion was considered too detailed for this review and the main points have therefore been summarised in table 3.

2.3. Application to intra-fraction motion estimation

2.3.1. Studies using US intra-fraction motion estimation. The first commercially available US based intra-fraction motion monitoring system, the Clarity Autoscan™ (figure 5) integrates a mechanically-swept 3D US transducer into the treatment planning (computed tomography (CT) suite) and delivery (treatment room) process. A 5 MHz transducer is positioned for transperineal prostate imaging. During treatment, 3D US images are acquired at 2.5 s intervals and registered to a reference US volume using a correlation-based search with reference ROIs centred on pixels within 2 cm of the prostate boundary. Phantom studies demonstrate that <1.2 mm accuracy and precision of motion estimation can be achieved using Clarity Autoscan™ (Abramowitz *et al* 2012, Lachaine and Falco 2013). Intra-fraction motion estimation of the prostate *in vivo* has yet to be compared to other techniques such as those based on x-ray imaging of fiducial markers (Ng *et al* 2012).

Other US intra-fraction motion estimation techniques being researched are listed in tables 4 and 5, many of which have been confined to phantom investigation (table 4).

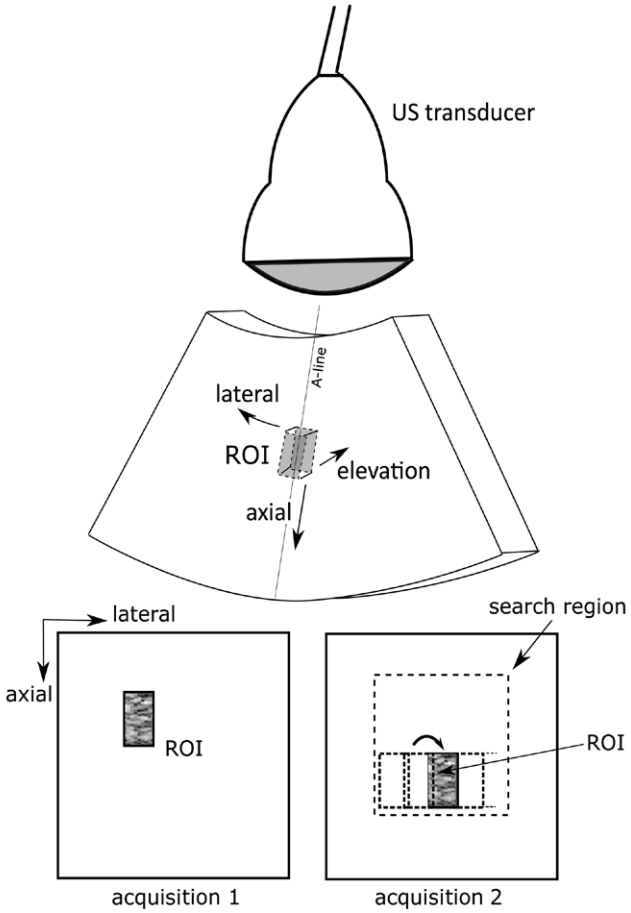

Figure 4. Example of 2D US echo pattern matching. A kernel or reference ROI is selected in an US image (acquisition 1) and the pattern that best matches this is located in a subsequent image (acquisition 2) by computing a similarity metric, such as the normalised cross-correlation coefficient, at many test locations within a larger search region. The top image illustrates a sector scan and the bottom two image acquisitions are assumed to be in polar coordinates, where the direction labelled lateral is measured in terms of the angle at which each A-line is acquired. The method can be extended to 3D if elevational data is available.

Some have evaluated the accuracy of intra-fraction motion estimation using ROIs containing resolved features (Abramowitz *et al* 2012, Schwaab *et al* 2014) and some with ROIs containing US speckle only (Sawada *et al* 2004, Hsu *et al* 2005, Harris *et al* 2007, O'Shea *et al* 2014).

Tissues investigated: A handful of *in vivo* studies (table 5) have shown the feasibility of 2D US-based motion tracking of the diaphragm (Xu and Hamilton 2006), liver (Jacso *et al* 2009, Rubin *et al* 2012), prostate (Schlosser *et al* 2010, Schlosser *et al* 2011) and lung surface (Rubin *et al* 2012). Liver motion estimation in 3D was demonstrated by Harris *et al* (2010). The pancreas can be difficult to visualise with an abdominal US transducer. Omari *et al* (2015) have assessed the feasibility of using portal vein motion, visualised using Elekta Clarity™, as a surrogate for pancreatic motion. US has not been used for intra-fraction motion estimation

Table 3. Factors influencing the accuracy of direct echo pattern matching motion estimation.

Factor		Effect	Potential solution(s)
Target specific	Rotation and deformation	Large inter-frame deformations (>5%) and rotations (>2°) limit accuracy of echo pattern matching (Kallel *et al* 1994, Meunier and Bertrand 1995, Bamber and Bush 1996, Fan *et al* 1997, Varghese and Ophir 1997, Meunier 1998, Brusseau *et al* 2000)	• Optimise trade-off between temporal resolution, spatial sampling and field-of-view. (Doyley *et al* 2001) • Including anatomical features in the ROI may increase maximum inter-image rotation/deformation. (Harris *et al* 2010) • Regularisation techniques using *a priori* data could improve results. (Cespedes *et al* 1997, Huang *et al* 2008, Gastounioti *et al* 2011, Bell *et al* 2012, O'Shea *et al* 2016)
	Direction of motion	The axial sampling interval is typically smaller than the lateral and elevational sampling intervals. Motion estimation was found to be most accurate in the axial direction (Harris *et al* 2007)	• Knowledge of specific organ motion and transducer spatial and temporal characteristics should be used to guide alignment of the transducer with respect to the patient axes (O'Shea *et al* 2014) • Use of matrix array transducer (Bell *et al* 2012)
	Object depth	For curvilinear transducers, spatial sampling interval increases with depth in the lateral and elevational directions. Motion estimation accuracy was observed to be poorer at greater depths (Harris *et al* 2007)	• Use sub-sample estimation (see below)
	Object speed	For mechanically swept transducers, the spatial sampling interval of objects moving retrograde to the sweep direction increases with increasing speed, resulting in a decrease in motion estimation accuracy. Speeds of up to 35 mm s^{-1} were observed to have no influence on the motion estimation accuracy in lateral direction (Harrington *et al* 2011, Harris *et al* 2011)	
Imaging data	Image data type	Radio frequency (RF) data can be used to measure much smaller displacements (tens of micrometres) than B-mode data (Bohs and Trahey 1991, Hein and O'brien 1993, Shi and Varghese 2007, Tavakoli *et al* 2010, Bamber *et al* 2013)	• Combined algorithms that use the envelope signal for estimating large motion and the RF signal to refine the estimate could be investigated. (Doyley *et al* 1996, Varghese and Ophir 1997)

(*Continued*)

Table 3. (*Continued*)

Factor		Effect	Potential solution(s)
		The envelope signal contains the echo signal features required to track large displacements (i.e. as in RT tumour motion), and may decorrelate less rapidly than the phase in the corresponding RF data. (Doyley *et al* 1996, O'Shea *et al* 2015)	
	Noise and artefacts	Direct motion estimation algorithms can suffer from decorrelation (between the reference and current image) when the image quality becomes poor due to e.g. random electronic or thermal noise (Bohs *et al* 1995, Yeung *et al* 1998), acoustic noise (Bohs *et al* 1995) or shadowing	• Automatic methods of shadow detection. (Noll *et al* 2014)
Motion estimation algorithm	Region of interest size	A large ROI contains a more unique echo pattern and will thus track motion with greater accuracy than would a small ROI (Ramamurthy and Trahey 1991, Morsy and von Ramm 1999)	• Updating the ROI size may provide a compromise between spatial resolution and accuracy (De Luca *et al* 2013) • Regularisation techniques using *a priori* data could improve results. (O'Shea *et al* 2016)
		A small ROI, however, provides the best spatial localisation (resolution) of the motion and smallest computational load	
	Fixed or incremental motion estimation	A fixed ROI may lose correlation and therefore accuracy for large displacements, the accumulation of small tracking errors (including interpolation bias errors) when incremental tracking is used may result in less reliable tracking (Matthews *et al* 2004, Harris *et al* 2010)	• Adaptive and regularised updating of the ROI appears to greatly improve incremental tracking performance (O'Shea *et al* 2016). Other techniques attempt to compensate for ROI drift (De Luca *et al* 2013)
	Sub-sample interpolation	Displacement sensitivity is limited by the sampling interval, which in the lateral and elevational (in 3D) directions is equal to the A-line and elevational frame density, respectively	• Interpolation of the similarity measure is a more computationally efficient method of improving displacement sensitivity compared to interpolating the echo imaging data. The grid slopes algorithm (Geiman *et al* 2000) was said to provide unbiased displacement estimates compared with cubic spline (Geiman *et al* 2000) and parabolic interpolation (Foster *et al* 1990). Others have used a Gaussian-shaped interpolator (Housden *et al* 2006)

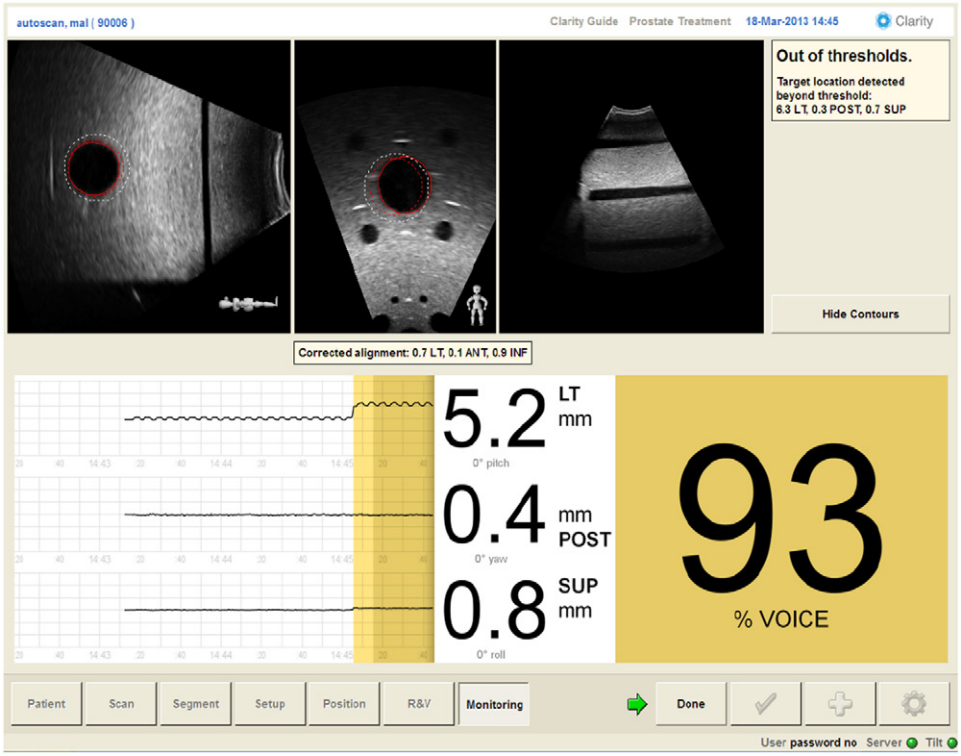

Figure 5. The Clarity Autoscan™ system with the monitoring interface showing a phantom used to simulate intra-fraction motion imaging. The dotted red contour is the reference target (reference planning volume, RPV). The solid red line indicates the current target contour. The dotted white line indicates the location of the VRV (VOICE reference volume). The % VOICE (volume of interest coverage estimate) is the percentage of target volume covered by the VRV contour (93% in this example). Courtesy of Martin Lachaine (Elekta Ltd).

for lung tumours, probably due to the high attenuation of US in lung and the success of optical monitoring of surface tumours. US monitoring of diaphragm motion could however be combined with surface motion to obtain a better estimate of lung tumour motion. Other abdominal tissues, such as bladder and kidney have yet to be studied clinically. The bladder is easily visualised on US and there is evidence to suggest that significant motion of the bladder wall may occur during therapy (McBain *et al* 2009a). Similarly, the kidneys are easily accessible by US and US-based motion estimation of the kidney may have application to SBRT of adrenal gland metastases (Chawla *et al* 2009) or in paediatric RT of the upper abdomen (Panandiker *et al* 2012). It is unlikely that US-based methods for estimating breast tissue motion hold great advantage over surface techniques.

Of the US intra-fraction motion estimation studies that employed *in vivo* data, comparison with the true motion (and therefore motion estimation accuracy) has either not been fully considered or has been based on manual annotations of features in B-mode images (e.g. De Luca *et al* 2013). There remains a need for full *in vivo* investigation of the accuracy and limitations of US-based methods, and therefore a need for improved methods for measuring the true motion. Comparison with other technologies such as kilo-voltage (x-ray) intra-fraction monitoring, which has shown acquisition rates (5–10 Hz) comparable with US and systematic accuracy

Table 4. Phantom-based studies of US-based intra-fraction motion estimation in RT. The transducer type, motion estimation method and main findings are included.

Site	Transducer	Motion estimation method	3D	Investigation/finding	Publication
Phantom	Not specified (3D)	Echo pattern matching	Yes	Respiratory gating using 3D US Results show synchronisation of phase of echo pattern matching (NCC) and periodic motion of organs such as the liver and pancreas	Sawada *et al* (2004)
Phantom	5 MHz, linear array	Echo pattern matching	No	Feasibility of US tracking with linear accelerator (linac) operating Minimal effect of transducer of dose distribution Negligible effect of linac on 2D echo pattern matching	Hsu *et al* (2005)
Phantom	4–7 MHz, curvilinear	Echo pattern matching	Yes	Dependence of echo pattern matching on depth, spatial samplIng, motion magnitude for known displacements of 1, 2 and 8 mm	Harris *et al* (2007)
Phantom	Not specified	CT to US image registration	No	Novel US-CT fusion system developed and tested CT image data superimposed on live US image System found to have sufficient accuracy for assessment of respiratory-induced tissue motion	Molloy and Oldham (2008)
Phantom	4–7 MHz, curvilinear	Echo pattern matching	Yes	Investigated the effect off object speed and direction on motion estimation accuracy Motion estimation errors in the elevational direction highlighted the limitations of 3D sweep transducers for respiratory motion	Harris *et al* (2011)
Phantom	5 MHz, microconvex 4D	Echo pattern matching	Yes	3D motion phantom tracked with Clarity Autoscan system and Calypso and optical system Calypso & optical: 95% of distance variation <0.6 mm, clarity auto-scan $\leqslant 1.3$ mm	Abramowitz *et al* (2012) (abstract only)
Phantom	5 MHz, microconvex 4D	Echo pattern matching	Yes	Accuracy of phantom displacements: 0.2, 0.0, 0.2 mm (AP, RL, SI)	Lachaine and Falco (2013)
Phantom	Not specified, biplane	Indirect method (contour)	Quasi	Biplane ultrasound probe used with active contouring to track 1D sinusoidal motion of rubber ball target Prediction used to account for imaging and motion estimation latency	Schwaab *et al* (2014)

(*Continued*)

Table 4. (*Continued*)

Site	Transducer	Motion estimation method	3D	Investigation/finding	Publication
Phantom	7.5 MHz, linear array	Echo pattern matching	Yes	Phantom displaced in 3D using prostate motion data from Calypso Tracked with US and kV x-ray system on CyberKnife Accuracy of 3D-US motion estimation comparable with kV xray for major axes of motion	O'Shea *et al* (2014)

Table 5. Application of US to *in vivo* intra-fraction motion estimation in RT. The site investigated, transducer type, motion estimation method and main findings are included.

Site	Transducer	Motion estimation method	3D	Investigation/finding	Publication
Diaphragm	Not specified	Echo pattern matching	No	Novel respiratory detection method based on diaphragm motion using four volunteers	Xu and Hamilton (2006)
Liver	Not specified	Echo pattern matching	No	US-gated liver radiation therapy feasibility study Temporal accuracy (lag) comparable with x-ray imaging system	Jacso *et al* (2009)
Liver	4–7 MHz, curvilinear	Echo pattern matching	Yes	Estimated motion compared with known sinusoidal motions. Four healthy volunteers Mean absolute devaition and SD of tracked vessels <1.7 mm Fixed reference tracking gave best results	Harris *et al* (2010)
Prostate	2.5 MHz, abdominal	Echo pattern matching	No	Could detect motion before prostate displaced by 3 mm or rotated by 5 degrees at 95% confidence level	Schlosser *et al* (2010)
Prostate	1–5 MHz, curved array	Echo pattern matching	No	Telerobotic system for real-time US imaging during radiation therapy	Schlosser *et al* (2011)
Prostate, Liver, Lung	2.5 MHz, phased array 6.0 MHz, Linear array	Echo pattern matching	No	Motion estimate versus human observer <2.0 mm difference	Rubin *et al* (2012)
Liver	2.8 MHz, 2D matrix array	Echo pattern matching	Yes	Liver ultrasound (three volunteers) to study scan rates with matrix array 12 Hz volume rate is needed to track respiratory motion with 1 mm RMS error	Lediju Bell *et al* (2012)
Liver	1.8–2.2 MHZ, not specified	Echo pattern matching	No	Scale adaptive block matching with temporal realignment to reduce accumulation of tracking errors	De Luca *et al* (2013)
Pancreas	5 MHz convex 4D	Echo pattern matching	No	Elekta Clarity used to track portal vein motion as surrogate for pancreatic motion	Omari *et al* (2015)

of <0.5 mm (Ng *et al* 2012), or with electromagnetic intra-fraction monitoring devices, e.g. *Calypso* (Willoughby *et al* 2006) (temporal resolution of 10 Hz, accuracy <0.5 mm), with appropriate EM shielding, may be astute.

2.3.2. Transducer type and imaging dimensions. While intra-fraction motion is inherently 3D, tissues generally exhibit greater motion in the superior-inferior and anterior–posterior motion directions. Left or right motion is often significantly smaller, making it less clinically relevant to RT. This supports the possible use of 2D images, as does low cost real-time imaging and the currently available high frame rate imaging. For example, 2D imaging could be performed with an appropriate left–right (RL) PTV margin to cover the expected magnitude of motion in the RL direction. This does, however, require the transducer to be aligned with the plane of dominant motion, and the development of methods for doing this rapidly and automatically. Direct comparisons of high frame-rate 2D US and slower volume rate 3D US for motion estimation of tissues have yet to be made. As an alternative to direct 3D US motion estimation, Preiswerk *et al* (2014) have combined 2D motion estimation and MRI-derived population-based motion models to estimate 3D displacement at high rates. The following considers the choice of transducer type, which may be 2D, 3D or biplanar.

2D transducers: A number of studies have investigated the use of 2D transducers for motion tracking in RT (e.g. Schlosser *et al* 2010, Schlosser *et al* 2011, Rubin *et al* 2012, see tables 4 and 5). Compared with 3D US, 2D monitoring decreases the (inter-image) computational load and, with smaller inter-frame displacement (due to higher frame rate), allows a smaller search window, further decreasing computation time. The high frame rate also helps to improve motion estimation by reducing inter-frame decorrelation in direct echo-based methods. At sufficiently high imaging rates (inter-frame elevation displacement <1 mm), and with a pre-calibration curve to convert decorrelation to distance (Bamber and Bush 1996, Chen *et al* 1997, Bush *et al* 2005, Housden *et al* 2007, Chen *et al* 2010), decorrelation can estimate out-of-plane motion enabling fast 3D motion estimation with a 2D transducer, albeit with potential elevation direction ambiguity. This method was adopted by Schlosser *et al* (2010), whereby a drop in the peak NCC value was used to indicate out-of-plane motion and rotation of the prostate during RT.

Biplanar transducers: Biplane imaging offers a high frame rate alternative to full 3D imaging whereby orthogonal imaging planes intersect. (e.g. Hossack *et al* 2001). Schwaab *et al* (2014) have investigated its use for RT intra-fraction motion compensation.

3D transducers: The advantages of direct motion estimation with 3D imaging over 2D, if the volume rate is high enough to avoid decorrelation due to rotation and deformation, are (i) the elimination of decorrelation (and consequent loss of tracking accuracy) due to out-of-plane motion, (ii) the unambiguous measurement of all 3 components of the displacement vector, (iii) the possibility to estimate rotations about three axes of rotation and deformation (e.g. Meunier 1998, Saito *et al* 2009) and (iv) a higher motion estimation precision due to the more unique speckle pattern (Morsy and von Ramm 1998). Unfortunately, mechanically swept 3D US transducers have low volume rate which limits their value for tracking relatively high velocity respiratory-induced motion (Harris *et al* 2011). Fully real-time (>20 Hz) 3D US imaging (Gunarathne 2013) is still at an early stage of development. Future methods may be based on 2D matrix array transducers, where the 3D volume rate is not limited by mechanically sweeping hardware (e.g. Harris *et al* 2011, Lachaine and Falco 2013, O'Shea *et al* 2014) and may reach several thousand Hertz (Byram *et al* 2010) with improved spatial resolution compared to that provided by equivalent 1D arrays. Bell *et al* (2012) used a 2D matrix array (operating at 48 Hz) for 3D liver motion estimation in RT, showing that volume rates of 12 Hz are need to accurately estimate cardiac and respiratory-induced liver motion.

2.3.3. Transducer placement. Intra-fraction estimation requires the US transducer to remain in contact with the patient throughout treatment. This presents a challenge: finding the transducer placement which allows adequate imaging quality without impacting negatively on the RT workflow.

Dosimetric impact: To date, the potential for a transducer positioned for minimum impact on the dose distribution to degrade target motion tracking has been studied only for skin contact scanning, where changes in the dose delivered to the target may be due to (i) RT beam attenuation when irradiating through the transducer (Bazalova-Carter *et al* 2015) and radiation scattering by the transducer when it is positioned at the radiation field edge, and (ii) modification of the RT beam angles to avoid the transducer (Wu *et al* 2006, Zhong *et al* 2013).

Using a RANDO® phantom and thermoluminescent detectors Hsu *et al* (2005) found that a transducer positioned for transabdominal prostate imaging resulted in only a 2.6% change (predominantly in surface dose) to the dose over the volume of the phantom from a single 10MV $10 \times 10\,\mathrm{cm}^2$ photon beam. Transperineal imaging of the prostate (with the transducer in a stationary holder e.g. Clarity Autoscan) has yet to be studied in this way, but for coplanar treatments should have limited impact along the radiation beam directions. Zhong *et al* (2013) used planning simulations and a virtual transducer to show that, with the exception of superficial targets, liver stereotactic body RT is feasible with the transducer parallel to the patient axis.

Irradiation through the US transducer, which strongly attenuates the RT beam, is not recommended (Bazalova-Carter *et al* 2015). To avoid this with a suitable margin, e.g. in VMAT treatment, a simple planning structure could be defined and a strict dose constraint applied to the block during trajectory optimization (similar to metal hip avoidance (Prabhakar *et al* 2013). For transabdominal prostate imaging, the dose-volume histogram (DVH) for a plan that avoided the transducer was in good agreement with the DVH of a clinically deployed plan (Schlosser *et al* 2010). The smaller the transducer, the less likely it will interfere with the treatment. As 3D and biplanar transducers are larger than 2D transducers this may be another reason to consider the latter. An alternative approach which uses a radiolucent mechanical scanning assembly containing a single element US transducer eliminates the majority of dense materials typically present in an electronically scanned US transducer array (Schlosser and Solek 2015).

Whilst wireless transducers (e.g. Siemens Acuson Freestyle™) hold potential for easier implementation, i.e. no US scanner next to the treatment couch, it is unlikely they will decrease the impact on the treatment plan. For certain treatment sites internal transducers (e.g. endorectal or endovaginal) would give the best spatial resolution and target tracking accuracy, due to short transducer to target distance. The dosimetric consequences of such transducer placement, and opportunities to include them in the planning process, need to be studied.

Robotic transducer positioning: Schlosser *et al* (2010) developed a telerobotic system to control the transducer position. The system was able to maintain the acquisition of high quality images over time periods relevant to treatment delivery in volunteers. It was also able maintain high quality transabdominal imaging during radiation delivery, robot performance and US target motion estimation of a phantom while a 15 MV beam was delivered.

In another robotic system (Sen *et al* 2015) the operator and robot share control of the US transducer, which helps to create a consistent body deformation from the force needed to make good contact between the transducer and the body. The system tracks the robot position and contact force used by the operator to obtain a reference US image during simulation, and uses virtual constraints to guide the operator to correctly place the transducer at treatment time. Studies of transducer placement are in progress for various abdominal sites, for both setup (inter-fraction) and delivery (intra-fraction motion) (e.g. Bell *et al* 2014).

2.5. Future developments

A number of developments and areas of research have the potential to make US a reliable option for intra-fraction tumour motion estimation:

(1) **Provision of real-time motion estimates**: Real-time *in vivo* US echo motion estimation was demonstrated for tissue strain imaging many years ago (e.g. Shiina *et al* 1996, Pesavento *et al* 2000, Hall *et al* 2003). Integration of real-time US and RT accelerator beam control systems via gating or tracking interfaces are in early stages of development (Schlosser *et al* 2010, Schwaab *et al* 2014, Gong *et al* 2015).

(2) **Automatic selection of tracking parameters and regularisation**: Pre-treatment imaging could train the motion estimator, which could also adapt to the target appearance (De Luca *et al* 2013). Substantial scope exists for improving echo pattern matching accuracy by further development of regularisation methods and their associated DQMs, particularly in 4D (Harris *et al* 2007, Bell *et al* 2012, O'Shea *et al* 2015), and by extending the methods to measure and account for rotation and deformation, for which optical flow (Duan *et al* 2009) could be studied as an alternative to similarity-based template matching. Other methods have used cost functions incorporating similarity of echo amplitudes and displacement continuity to regularise displacement estimation (Rivaz *et al* 2008, Jiang and Hall 2009). A novel 3D prostate US segmentation algorithm using patch-based anatomical features and support vector machines has recently been presented and has potential for extension to intra-fraction motion estimation (Yang *et al* 2015).

(3) **Clinical validation**: The need for *in vivo* validation was discussed above. The effect of transducer placement on the trade-off between motion estimation (dependent on image quality) and impact on the dose distribution should be fully explored using conventional and novel transducer designs.

(4) **Application to other treatment sites**: While currently only applied to intra-fraction motion estimation of the prostate, US could be highly beneficial for other abdominal sites such as the pancreas, kidney, uterus and cervix (table 1). A combination of inter- and intra-fraction motion estimation using US could compensate for bladder and rectal motion, and enable reduced PTV margins in the lower pelvic region. Stereotactic body radiation therapy (SBRT) with compensation for respiratory motion is becoming a standard for treatment of primary and metastatic liver tumours (Schefter *et al* 2005, Mancosu *et al* 2012). Likewise, the kidney, which limits RT dose to abdominal sites such as adrenal tumours (Dawson *et al* 2010, Scorsetti *et al* 2011), can undergo relatively large respiration induced intra-fraction displacement (Langen and Jones 2001). The non-ionising nature of US guidance might be particularly beneficial to paediatric patients (Panandiker *et al* 2013) by reducing secondary cancer risks.

3. US techniques for target definition, monitoring tumour response and assessing normal tissue toxicity

The tumour visualised using anatomical imaging may not always represent the desired biological target volume (BTV) (Ling *et al* 2000), the definition of which requires additional knowledge about the cells, such as their state of proliferation and oxygenation (Nestle *et al* 2009). For example, regions of hypoxia, associated with radio-resistance (Zahra *et al* 2007) have been shown to influence response to RT (Vergis *et al* 2008). The tumour microvasculature, therefore, plays an important role in RT (Kim *et al* 2006). Research is underway to develop and employ functional and molecular imaging to define the BTV and measure its changes during treatment.

Such techniques have been reviewed (Nestle *et al* 2009, Bussink *et al* 2011) and have potential for integration into the RT workflow (Munley *et al* 2013) for monitoring tumour response (Brindle 2008, Horsman *et al* 2012) or normal tissue (toxic) reactions (Jeraj *et al* 2010) to RT. MR is increasingly used for these purposes (Postema *et al* 2015b) for example, in the delineation of the dominant intraprostatic lesion prior to prostate boost RT (Riches *et al* 2014). The introduction of US into the RT suite brings potential to use US functional and molecular imaging for these purposes. Not only is US easily affordable, it could provide images at many time points during RT. Currently functional MR, CT and PET imaging requires the patient to be removed from the RT couch to an imaging suite, which loses the real-time capability, adds significantly to treatment time, which may not be tolerated by a large fraction of patients, and degrades geometrical registration between imaging and treatment.

3.1. US imaging and measurement of tissue characteristics

Here we briefly review selected US imaging techniques which have potential for improving BTV definition, monitoring tumour response to RT and quantifying normal tissue toxicity. Table 6 gives a list of the US characteristics that may be measured using these techniques.

3.1.1. US backscatter characterisation of tissue. US backscatter characteristics (UBCs), as with other forms of ultrasonic tissue characterisation (TC) (Lerski *et al* 1981, Linzer and Norton 1982, Waag 1984, Greenleaf 1986, Insana *et al* 1988, Shung and Thieme 1992), are related to properties of US scatterers, e.g. scatterer size, density, spatial organization and relative acoustic impedance (Lizzi *et al* 2003). They may be used to detect morphological changes in tissue at the cellular level, and to identify disease (Feleppa *et al* 2004) for target volume delineation and tissue damage, such as cell death caused by RT (Lee *et al* 2012), for monitoring treatment response. UBCs can be derived using:

(1) *first-order statistical analyses of the echo amplitudes*. For examples see rows 1 to 4 in table 6 (Mountford *et al* 1973, Lerski *et al* 1981, Nicholas *et al* 1986, Bamber 1992, Bamber 1997, Bamber 1998, Hill *et al* 2004).
(2) *higher-order statistical analyses of the echo amplitudes*. See row 5, table 6 (Lizzi *et al* 1983, Wagner *et al* 1983, Bamber and Nassiri 1985, Nicholas *et al* 1986, Valckx and Thijssen 1997).
(3) *spectral analysis of RF echoes (backscatter spectroscopy)*. Features of averaged spectra may be derived from a regression analysis of the normalized Fourier transform of the RF echo signal, and include the mid-band fit (MBF), US integrated backscatter (UIB), spectral slope (SS) and spectral intercept (SI) (O'Donnell and Miller 1981, Lizzi *et al* 1983, Feleppa *et al* 1986), as shown in figure 6.

3.1.2. Doppler and contrast enhanced US. Colour Doppler US (CDUS) imaging, power Doppler US (PDUS) imaging and spectral Doppler US measurement (reviewed by, for example, Evans *et al* 2000, Eckersley and Bamber 2004) are not truly quantitative techniques, being limited by factors such as Doppler signal angle and depth dependence (Bamber *et al* 2013). Nevertheless, a large body of work has demonstrated the value of relative characteristics such as those listed in table 5 as non-invasive measures of tumour blood flow and vascularisation (Minasian and Bamber 1982, Wells *et al* 1997).

Changes in the microvasculature at the capillary level (<100 μm) may occur early in response to treatment (Brown 2002). Intravenously injected gas-filled microbubbles (e.g. Goldberg *et al* 2001, Stride 2008) of ~1–8 μm diameter can be detected with excellent

Table 6. Selected US tissue properties and their RT applications (The table omits many US tissue properties; only those used in RT research have been listed).

Measured characteristics discussed in this review (alternative names)	Description	Units	Applications discussed in this review	Publications[a]
Ultrasound backscatter characterization:				
Relative US backscatter amplitude (echogenicity)	Mean echo amplitude	dB	Imaging apoptosis (PC)	Czarnota *et al* (1999)
			Assessment of RT toxicity (C)	Ying *et al* (2007)
Skewness	Pixel histogram skewness		Prostate cancer imaging	Houston *et al* (1995)
Kurtosis	Pixel histogram kurtosis		Prostate cancer imaging	Houston *et al* (1995)
Relative peak intensity value	Peak value of echo amplitude histogram	dB	Assessment of RT toxicity (C)	Yang *et al* (2012)
Lateral autocorrelation	Mean correlation between pairs of adjacent A-lines		Assessment of RT toxicity (C)	Lui *et al* (2010)
Mid band fit (MBF) (ultrasound integrated backscatter (UIB))	See figure 6	dB	Tumour response to RT (C)	Vlad *et al* (2009)
			Assessment of RT toxicity (C)	Zhou *et al* (2009)
			Imaging apoptosis (PC)	Czarnota *et al* (1999)
Spectral slope (SS)	See figure 6	dB MHz^{-1}	Assessment of RT toxicity (C)	Vlad *et al* (2009)
Spectral intercept (SI)	See figure 6	dB	Assessment of RT toxicity (C)	Vlad *et al* (2009)
Colour and power Doppler ultrasound:				
Colour or power area	Total area of coloured pixels	m^{-1}	Measurement of tumour vascularity (PC)	Donnelly *et al* (2001) Kim *et al* (2006)
Colour pixel density (CPD) (power and colour)	Area of colour pixels/total ROI area		Measurement of tumour vascularity (PC)	Niizawa *et al* (2005), Kim *et al* (2006)
			Measurement of tumour vascularity (C)	Hwang *et al* (2010)
			Measurement of tumour hypoxia (PC)	
Vascularity Index (VI)	Integrated power in ROI / total ROI area	dBm^{-2}	Measurement of tumour vascularity (PC)	Huang *et al* (2013)
			Assessment of RT toxicity (C)	
Mean Power (or velocity)	Total power (or velocity) in ROI/ Area of colour pixels (power is related to blood volume)	dB m^{-2} (m^{-1} s^{-1})	Measurement of tumour vascularity (PC)	Fleischer *et al* (1999)

(*Continued*)

Table 6. (*Continued*)

Measured characteristics discussed in this review (alternative names)	Description	Units	Applications discussed in this review	Publications[a]
Spectral Doppler ultrasound:				
Peak systolic velocity (PSV)[b]	Maximum blood velocity in the systole phase	m s^{-1}	Assessment of RT toxicity (C)	Bakhshandeh *et al* (2012)
End diastolic velocity (EDV)[b]	Blood velocity at end of the diastolic phase	m s^{-1}	Measurement of tumour vascularity (C)	Ahuja *et al* (1999)
Resistance index (RI)	(PSV − EDV)/mean velocity		Measurement of tumour vascularity (C) Assessment of RT toxicity (C)	Ahuja *et al* (1999)
Pulsatility index	(PSV − EDV)/EDV		Measurement of tumour vascularity (C)	Huang *et al* (1996), Ahuja *et al* (1999)
			Assessment of RT toxicity (C)	Bakhshandeh *et al* (2012)
Dynamic contrast enhanced (DCE) ultrasound:				
Area under the curve (AUC)	Area under the time intensity curve (TIC) related to total vascular volume of the ROI	dBs	Measurement of tumour hypoxia (C)	Scholbach *et al* (2005)
Peak intensity (I_p)	Maximum intensity in the wash in curve	dB	Measurement of tumour vascularity (PC)	Hwang *et al* (2010)
			Measurement of tumour vascularity (C)	Krix *et al* (2005)
Time to peak (t_p)	Time from zero intensity (before contrast arrives) to peak intensity	s	Measurement of tumour vascularity (PC)	Elie *et al* (2007)
Mean transit time (MTT)	Mean time taken by the contrast to pass through the ROI	s	Measurement of tumour vascularity (PC)	Elie *et al* (2007)
Elastography:				
Strain	Axial strain, a measure of tissue deformation showing contrast for relative shear modulus and other biomechanical properties	%	RT target localization (C) Assessment of RT toxicity (C)	Rivaz *et al* (2009) Adriaenssens *et al* (2012)
Shear wave speed	Speed of shear waves (may be converted to elastic shear modulus)	m s^{-1} (kPa)	Tumour response to chemo-RT (C) Assessment of RT toxicity (C)	Rafaelsen *et al* (2013) Badea *et al* (2013)

[a] References provide examples where these characteristics have been applied directly to RT. If no RT related work exists, the references given are discussed in this review.
[b] Velocity cannot be measured in distributed tumour vasculature due to lack of knowledge of the Doppler angle, but it may provide useful measures of blood flow. See text for further discussion.
Key: PC—Preclinical study. C—Clinical study.

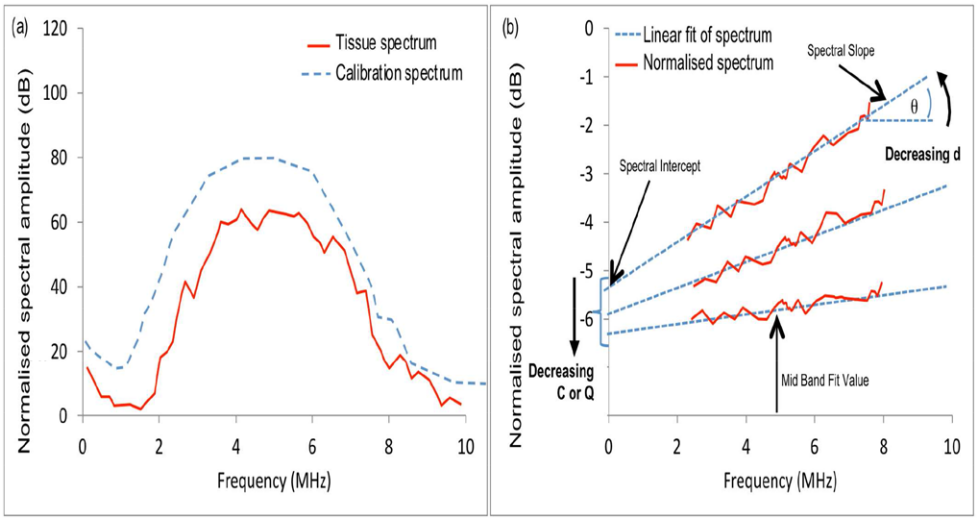

Figure 6. US backscatter characterisation by spectral analysis of the RF echo signal (Lizzi *et al* 1983). (a) Hypothetical attenuation-corrected tissue spectrum and calibration spectrum. A normalised amplitude spectrum (b) is obtained by dividing the tissue spectrum by the calibration spectrum. The dashed line shows a logarithmic fit, the slope and zero frequency intercept of which are the SS and SI, respectively. The MBF is the value of the logarithmic regression line at the center frequency, f_c, of the spectral band. Another feature used is the area under the curve in (b), or UIB. Decreasing scatterer size, d, results in an increase in SS, and (depending on the ratio of scatterer size to wavelength within the spectral band) a decrease in SI, MBF and UIB. Decreasing scatterer density C, or the fractional difference between the scatterers' acoustic impedance and that of the background Q, results in a decrease in SI, MBF and UIB.

background tissue echo suppression by using nonlinear microbubble-specific US imaging modes, such as pulse-pulse phase and/or amplitude modulation (e.g. Stride and Saffari 2003, Qin *et al* 2009). In combination with temporal maximum intensity projection (MIP) imaging, such methods produce US 'angiograms' of tumour vasculature (figure 7) and microvasculature (Shelton *et al* 2015).

Tumour perfusion characteristics can be measured by analysing the kinematics of microbubbles in vessels as small as ~40 μm, using dynamic contrast-enhanced US (DCE-US) (e.g. Piscaglia *et al* 2012, Saini and Hoyt 2014). Clinical microvascular flow imaging with Doppler is becoming possible without a contrast agent. For example, 'Superb microvascular imaging' (SMI), offered by Toshiba on the Aplio500, is said to use advanced clutter reduction to enhance Doppler SNR. Using ultrafast frame rates (tens of kHz) Tanter and Fink (2014) employed massive averaging to enhance Doppler SNR, which has been used, for example, to visualise microvascular 'activity waves' propagating within the brain (Osmanski *et al* 2014). Ultrafast imaging also provides more time for US beam steering, to estimate the 2D (and eventually 3D) blood velocity vector, allowing complex flow patterns to be imaged (Hansen *et al* 2009), a technique with potential for more accurate characterisation of tortuous tumour vasculature. A new method of analysing DCE-US data, to assess spatial dispersion of time-intensity curves, has potential to improve prostate cancer detection (Schalk *et al* 2015), which may eventually be applicable to improving target delineation in RT. Finally, at appropriate microbubble concentrations, signals can be localised from spatially isolated microbubbles,

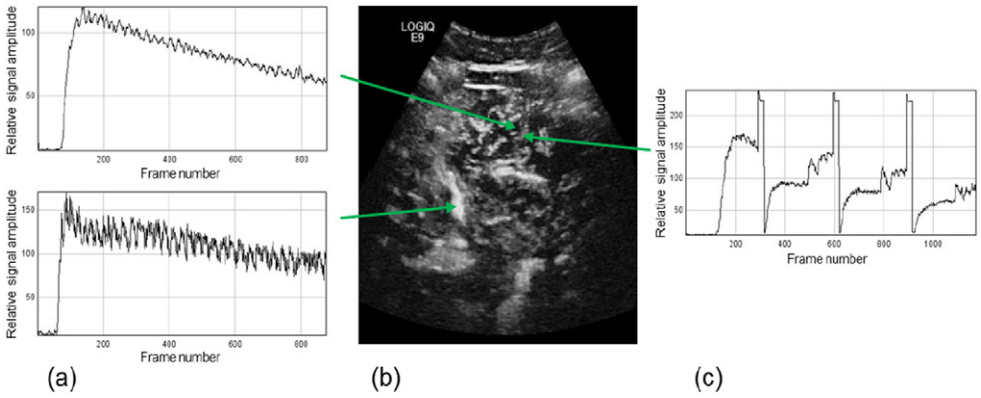

Figure 7. An example temporal maximum intensity projection (MIP) contrast image (b) shows a slice through the vascular architecture of a large liver metastasis. DCE-US is illustrated in (a), where the bolus time-intensity curves are from two example locations, a region of diffuse vasculature (upper) and a large vessel (lower, showing greater respiratory motion artefact), as indicated by the green arrows. DCE-US time-intensity curves for three destruction-replenishment sequences within a bolus contrast period from the diffuse vascular location are provided in (c). Definitions of DCE-US characteristics shown in table 6, and methods for measuring them from time-intensity curves, may be found in Dietrich *et al* (2012). The distance from the transducer to the maximum depth in the MIP image is 15 cm. (Image and graphs shown with thanks to N Tunariu and J Fromageau for assistance with data acquisition.)

which facilitates the potential for super-resolution (<10 μm) microvascular imaging (Desailly *et al* 2013, Viessmann *et al* 2013, Christensen-Jeffries *et al* 2014).

3.1.3. US molecular imaging (USMI) using contrast agents. Microbubbles conjugated to targeting molecules such as peptides or antibodies allow USMI (e.g. Wen *et al* 2014) of circulating molecules or those associated with endothelium such as vascular endothelial growth factor receptor type 2 (VEGFR-2) (Korpanty *et al* 2007, Rychak *et al* 2007) and α_v-integrins (Kiessling *et al* 2012). Liquid phase-change nanodroplets may allow extravascular molecular targeting but they are at an early stage of development (Wilson *et al* 2013). Another future option may be protein-shelled gas nanovesicles (GVs) extracted from microorganisms such as bacteria which produce GVs to control their buoyancy. These GVs provide stable US contrast, detectable *in vivo* with various useful properties as molecular reporters (Shapiro *et al* 2014). Most USMI work at present is pre-clinical, e.g. for assessment of tumour angiogenisis and response to anti-angiogenic therapies, although initial clinical studies are now underway in prostate (NIH 2015a, NIH 2015b, Kaneko and Willmann 2012).

3.1.4. US Elastography. US elastography aims to display contrast for, or quantities related to, the shear elastic moduli of tissue (Bamber *et al* 2013). The available techniques (e.g. Parker *et al* 2011, Bamber *et al* 2013, Doyley and Parker 2014, Shiina *et al* 2015) use methods described in section 2.2.1, such as similarity search or Doppler, to measure the temporal and spatial dependence of tissue displacement associated with the shear deformation of tissue, which can be used to infer, or quantify, tissue elasticity. Qualitative measures of elasticity strain and displacement are provided by strain elastography (SE) and acoustic radiation force impulse (ARFI) imaging, respectively. Methods giving quantitative elasticity measures (e.g. shear-wave speed, c_s, related to Young's Modulus, E, by $E = 3\rho c_s^2$, where ρ is the mass density) include transient, vibrational

and shear-wave elastography (TE, VE and SWE, respectively). For a detailed explanation of these techniques please refer to (Bamber *et al* 2013, and Shiina *et al* 2015).

For RT, elastography may improve the ability to visualise disease for target delineation (see section 3.2). Furthermore, as elastography is sensitive to tumour cell necrosis (Li *et al* 2014), oedema (Berry *et al* 2008) and fibrosis (Bush *et al* 2005), and as tissue elasticity is affected by RT (Yarnold and Brotons 2010), it is plausible that elastography may be used to monitor tumour response and normal tissue toxicity. Finally, as tissue viscoelasticity has been shown to be associated with both fibrosis (Cosgrove *et al* 2013, Ferraioli *et al* 2015) and microvessel density (Jugé *et al* 2012, Jamin *et al* 2015), and fibrosis is linked with induction of angiogenesis via hypoxia inducible factors (HIF) (Ruthenborg *et al* 2014), it is conceivable that elastography may help define the BTV. This hypothesis has yet to be tested.

3.1.5. Photoacoustography. Photoacoustic imaging (PAI) (Wang 2009) uses pulsed light to induce a transient (<10 ns) temperature and pressure rise wherever the light is absorbed, typically in haemoglobin, melanin and, to some extent, fat. This generates acoustic emissions detectable by an US transducer, providing real-time imaging of the optical absorption properties of tissue. Although imaging depths of up to 7 cm have been reported (Zackrisson *et al* 2014), the reliability of the image detail at such depths depends on whether image clutter is generated by strong photoacoustic sources outside the imaged region, and methods of distinguishing clutter from reliable detail are under development (Jaeger *et al* 2012, Jaeger *et al* 2013, Alles *et al* 2014). In different forms, PAI spectroscopy (Wang 2009), allows (a) molecular identification of endogenous chromophores or exogenous contrast in the form of dyes or nanoparticles which may be molecularly directed to extravascular targets (Wilson *et al* 2013, Zackrisson *et al* 2014); or (b) a PAI analogue of US backscatter spectroscopy (section 3.1.1) which permits absorber (e.g. microvessel) size, spacing and spatial organisation to be measured (Gertsch *et al* 2010, Preisser *et al* 2013, Xu *et al* 2014, Li *et al* 2015). Most PAI studies have been preclinical or have used tomographic systems (e.g. for imaging the breast), although translation to the clinic using hand held US transducers is underway (e.g. Wang *et al* 2011, Jaeger *et al* 2012, Alles *et al* 2013, Montilla *et al* 2013).

3.2. Improving target localisation for RT planning

It is clear that elastography can substantially increase US detection of prostate cancer (e.g. Teng *et al* 2012, Boehm *et al* 2015, Correas *et al* 2015, Hwang and Lee 2014, van Hove *et al* 2014), and the potential was highlighted in sections 3.1.2 and 3.1.3 in this respect, for DCE-US and molecular targeted microbubbles. Two groups have considered using US for improved dominant intra-prostatic lesion (DIL) detection for guiding external beam RT: Walz *et al* (2011) and Zhang *et al* (2007). Walz *et al* (2011) reported sensitivity and specificity of SE to be low at 59% and 43%, respectively. In the context of DIL detection for prostate biopsy guidance, higher values have been reported for B-mode, Doppler and DCE-US (reviewed by Postema *et al* 2015b). Zhang *et al* (2007) performed a theoretical risk-benefit analysis of 3D image guided dose painting using imaging transrectal B-mode US and UBC.

There is a need for side-by-side comparisons of the different US techniques, to determine which performs best, or whether an integrated approach would be worthwhile, as has been suggested for prostate biopsy guidance (Brock *et al* 2013, Postema *et al* 2015a, 2015b). Multi-parameter MRI (mMRI) is widely considered a gold standard for intra-prostatic lesion detection (Khoo and Joon 2014). Comparison of US techniques, or a multi-parameter US approach, with multi-parametric MRI, in the prostate biopsy setting may provide strong evidence for the application of US methods to prostate tumour delineation.

Poor CT soft tissue contrast limits the accuracy of tumour bed delineation for patients receiving breast boost RT post-surgery (Coles *et al* 2007). In a proportion of patients, a pocket of fluid, or seroma, is present, which may be accompanied by surgery related scar tissues (Mukesh *et al* 2012). Seroma can be visualised using B-mode US, as discussed in Fontanarosa *et al* (2015), but other tissues, such as scar tissue surrounding the tumour bed, are not easily differentiated from fibroglandular tissue. Rivaz *et al* (2009) showed using SE that elastographic contrast between seroma (fluid) and fibroglandular tissue was significantly greater than radiographic contrast obtained using CT. Juneja *et al* (2014) compared SE and SWE for TB delineation in US breast phantoms, finding SE gave a more accurate representation of inclusions.

3.3. Tumour response to treatment

3.3.1. Measurement of cell death. US backscatter spectroscopy (section 3.1.1(3)) has been investigated at high frequencies (>20 MHz) for monitoring radiation-induced apoptosis *in vitro* and in small animal models (Czarnota *et al* 1999, Vlad *et al* 2009), with validation against histopathology (Czarnota *et al* 2007). Its clinical feasibility to monitor response of deep-seated tumours has yet to be proven, although reason to be optimistic is provided by the ability of the method at low frequencies to characterise microscopic structure in phantoms (e.g. Insana *et al* 1990) and, for example, to identify glomeruli as one of the dominant scattering structures in the renal cortex (Insana *et al* 1991).

3.3.2. Measurement of tumour vascularity. PDUS and DCE-US have been investigated pre-clinically to quantify tumour response to RT, although some groups found high positive correlation of Doppler characteristics with histologically assessed microvessel density pre- and post-RT (Donnelly *et al* 2001, Kim *et al* 2006), whereas others did not (Fleischer *et al* 1999, Denis *et al* 2002, Hwang *et al* 2010). Hwang *et al* (2010) and Krix *et al* (2003), however, did report a strong correlation of DCE-US I_p with MVD. Finally, the PDUS vascularity index has been noted to decrease in tumours treated with US and microbubbles (see section 3.3.3), alone or with radiation (Czarnota *et al* 2012, Tran *et al* 2012).

Clinically, a significant reduction in pulsatility and resistance indices of the intranodal vessels of metastatic lymph nodes (see table 5) 8 weeks post-RT was demonstrated (Ahuja *et al* 1999). Pirhonen *et al* (1995) found RT caused a significant decrease in cervical tumour vascularity during treatment, which was associated with disease free survival. Huang *et al* (2013) demonstrated a 50% reduction in 3D PDUS vascularity index, 5 weeks from start of RT, dropping to 100% reduction at 3 months, in women receiving RT or concurrent chemoradiotherapy for cervical carcinoma. Krix *et al* (2005) observed a decrease (~20%, larger than measured using contrast-enhanced CT) in tumour arterial phase DCE-US I_p 2 months after single fraction stereotactic body RT to liver metastases. Following proton therapy of hepatocellular carcinoma, contrast enhanced CDUS tumour CPD initially increased in 50% of patients and then, 9 months post-RT, decreased across all patients (Niizawa *et al* (2005).

Further work and greater standardisation of techniques are required to understand how Doppler US and DCE-US characteristics relate to tumour vasculature and perfusion. An inherent difficulty in histological evaluation of tumour response both clinically and pre-clinically is establishing accurate spatial registration between histological sections, dose distribution and the US imaging plane. Three-dimensional US, provides more accurate image registration compared to 2D (Hwang *et al* 2010, Huang *et al* 2013). Pre-clinically, integration of functional 3DUS into small animal dedicated irradiation devices may bring about increased accuracy in correlative studies of this kind (Verhaegen *et al* 2011).

3.3.3. Manipulation of tumour vasculature. Although US has long been studied as a technique for inducing hyperthermia (Hand and Haar 1981), and hyperthermia and RT are known to act synergistically (e.g. Miller *et al* 1977, Holt 1980), the potential for synergism between therapeutic US methods for example high intensity focused ultrasound (HIFU) (Baker *et al* 2001, Tachibana 2004, Koonce *et al* 2015, Wood and Sehgal 2015) and RT has only just begun to be investigated, and only in a preclinical context. The induction of endothelial cell apoptosis by exposure to US in the presence of microbubbles is proposed as a possible mechanism for observed radioenhancement (Al-Mahrouki *et al* 2012), and a ten-fold increase in tumour cell-kill was observed using a combined treatment relative to microbubbles or radiation alone (Czarnota *et al* 2012, Tran *et al* 2012). Furthermore, US contrast-mediated vascular permeation and drug delivery (Rapoport *et al* 2007) holds potential for the localised delivery of radiosensitisers such as Paclitaxel (Liebmann *et al* 1994) or epidermal growth factor receptor inhibitors (Sartor 2004).

3.3.4. Measurements of tumour oxygenation. Tumour hypoxia has been shown to be associated with a decrease in vascularity (West *et al* 2001) motivating research into Doppler and DCE-US characteristics as markers of hypoxia, validated against measures of oxygen partial pressure (pO_2) using polarography. Clinically, Scholbach *et al* (2005) and Gagel *et al* (2007) reported moderate correlation with a tissue perfusion index (see table 6) and polarographic measurements in metastatic lymph nodes, respectively. Pre-clinically, weak (Ohlerth *et al* 2010) or no correlation (Elie *et al* 2007) with Doppler US characteristics was found. Poor results may have been a manifestation of problems with various factors in these types of experiment, viz., reliability of polarography *in vivo* and spatial sampling error of both polarography and US.

Using photoacoustography, Sun *et al* (2012), measured increases in tumour volume, and decreases in blood concentration and oxygen saturation, in tumour models irradiated with 30 Gy, comparing measurements taken before and 10 d post-irradiation. Similar findings, in response to US and microbubble enhanced RT, are reported by Briggs *et al* (2014).

3.3.5. Measurements of tumour stiffness. Limited clinical evidence to support the use of elastography to measure response to RT exists. Mabuchi *et al* (2015) using real-time SE, found that in patients with complete response, tumour stiffness decreased to levels similar to normal cervix. Rafaelsen *et al* (2013) detected a significant decrease in shear wave speed in rectal tumours and mesorectal fat, between baseline measurements prior to the start of chemoradiation therapy ($3.13\,ms^{-1}$) and two ($2.17\,ms^{-1}$) and six ($2.11\,ms^{-1}$) weeks after treatment began. A softening of metastatic cervical lymph nodes post-chemoradiation therapy was demonstrated using SE (Furukawa and Furukawa 2010).

3.3.6. Measurements of molecular biomarkers for RT response. The potential for USMI to measure response to RT has been demonstrated pre-clinically: microbubbles targeted to ICAM-1 (a marker of inflammation) and $\alpha_v\beta_3$-integrin (a marker of angiogenesis) allowed 30 MHz US to image early vascular response of xenograft prostate tumours irradiated with carbon ions, suggesting an increased expression of ICAM-1 and $\alpha_v\beta_3$-integrin in response to RT (Palmowski *et al* 2009). Gold nanorods with resonance peaks at 700 nm and 900 nm were functionalised with antibodies targeted to HER-2 and EGFR transmembrane receptors (Shah *et al* 2014) demonstrating potential for contrast photoacoustic stratification of tumours prior to therapy.

3.4. Assessment of normal tissue toxicity

Research investigating US quantification of normal tissue toxicity of RT is described below according to the normal tissue structures at risk from RT.

3.4.1. Salivary glands (head and neck RT). Xerostomia is a common complication of dose to the salivary glands during head and neck RT (Eisbruch *et al* 2001). On B-mode US, parotid glands become more heterogeneous and hypoechoic post-RT (Ying *et al* 2007, Cheng *et al* 2011). Significant differences in UBC (Yang *et al* 2012, Imanimoghaddam *et al* 2012), spectral Doppler characteristics (Ying *et al* 2007, Wu *et al* 2011), and shear wave speed (Badea *et al* 2013) between irradiated and non-irradiated tissue have been observed in parotid or submandibular gland, although Imanimoghaddam *et al* (2012) saw no difference in spectral Doppler characteristics between baseline and 6 to 7 week post-RT. No study has examined the spatial distribution of US characteristics; this may be of particular interest for trials of parotid sparing (Chao *et al* 2001) which aim to spare the region of the parotid containing stem cells.

3.4.2. Neck tissue (head and neck RT). In patients receiving head and neck RT, Leung *et al* (2002) detected significant differences (~25%) in subjectively estimated relative Young's modulus between regions of the neck receiving boost irradiation and those that did not. Zheng *et al* (2000) showed that skin thickness, MBF and SI of neck tissue significantly differed between patients following head and neck RT and healthy volunteers.

3.4.3. Normal breast tissue (breast RT). Women undergoing adjuvant RT for breast cancer may experience breast swelling (oedema), an acute effect, and breast hardening (thought to be associated with fibrosis), a late effect (Yarnold *et al* 2005). Yoshida *et al* (2012) measured skin thickness, subcutaneous tissue lateral correlation (see table 5) and MBF, in the irradiated and un-irradiated breasts of breast cancer patients post-RT (Liu *et al* 2010). Patients with acute (<6 months) radiation toxicity had significant differences between breasts in all three characteristics. Those with late (>6 months) Radiation Therapy Oncology Group (RTOG) grade 1 or 2 skin toxicity (RTOG 2015) had greater skin or subcutaneous tissue US characteristics compared to patients with RTOG grade 0 skin toxicity.

B-mode US has been used to measure an increase in skin thickness ($p < 0.001$) and relative US backscatter amplitude of subcutaneous tissue ($p \leqslant 0.05$) post surgery and RT (Adriaenssens *et al* 2012). SE was used to measure a decrease ($p < 0.05$) in subcutaneous tissue stiffness in patients approximately 10 weeks post RT compared to pre-surgery (Adriaenssens *et al* 2012) and an increase in stiffness in the irradiated breasts of women with late toxicity compared to the unirradiated breast (Bush *et al* 2005).

3.4.4. Heart (breast RT). The risk of heart disease subsequent to RT increases with mean heart dose (Darby *et al* 2013). Erven *et al* (2011) used strain rate imaging to show that left-sided breast cancer patients had a significant decrease ($p < 0.001$) in myocardial strain post RT ($17.6 \pm 1.5\%$) and 2 months follow-up ($17.4 \pm 2.3\%$) compared to pre-RT ($19.5 \pm 2.1\%$). No decrease in strain rate could be observed in segments that received less than 3 Gy but this may be due to the sensitivity of the technique rather than a lack of effect (Darby *et al* 2013).

3.4.5. Other tissues. In patients receiving RT for head and neck cancer, spectral Doppler PI, RI, and PSV of the inferior thyroid artery underwent significant changes by fraction 10 of RT, and mean relative US backscatter amplitude and heterogeneity of the thyroid gland decreased

(Bakhshandeh *et al* 2012). Krix *et al* (2005) showed that post-RT arterial phase DCE-US peak intensity increased in liver metastases suggesting radiation-induced hypervascularisation and support for the hypothesis that radiation-induced liver disease is a result of liver venous obstruction.

4. The use of US in 3D dosimetry

Accurate, cost effective, patient-specific 3D dose verification and validation tools are needed for verification of IMRT and arc RT. Available techniques include the reconstruction of 3D dose from portal images (van Elmpt *et al* 2008), 3D electronic dosimeters (e.g. Bedford *et al* 2009) and 3D plastic radiochromic dosimetry with optical CT read-out (e.g. Thomas *et al* 2011). Each has its disadvantages for routine use, and new approaches are required to verify future developments such as real-time adaptive RT that compensates for translational motion, deformation and rotation of the target between fractions and during irradiation (Landry *et al* 2015).

In addition, a direct experimental determination of dose *in vivo* would represent a major step forward, allowing real-time treatment adaptation of the dose distribution (Ziegenhein *et al* 2012). Various methods have been explored, such as PET imaging of hadron beam generated positron activity (Chatterjee *et al* 1981, Parodi *et al* 2002) and prompt gamma emission (Polf *et al* 2009), but none are, as yet, in wide clinical use.

US methods can be applied to 3D dose verification, and may provide advantages over the current techniques both in the clinic and for use in measuring national standards of dose. US methods for *in vivo* dosimetry, although more speculative, have received recent attention, especially for hadron and heavy ion therapy.

4.1. Verification using gel dosimetry

Two types of gel-based dosimeter have been investigated (table 7): (i) Fricke gel dosimeters (Schreiner 2004) and (ii) polymer gel dosimeters (Baldock *et al* 2010). Polymer gels that change their US properties on exposure to ionising radiation may in principle take advantage of the widespread availability of inexpensive US systems with high spatial resolution, which is important for resolving dosimetric properties such as a narrow (~1 mm) Bragg peak in hadron beams (Zeidan *et al* 2010). Alternative MRI (Maryanski *et al* 1994) or optical CT (Hilts *et al* 2005, Doran 2009) based systems may be expensive, time-consuming, or require new and dedicated imaging systems with limited sample size or resolution.

Common US gel formulations include polyacrylamide gel ('PAG') and methacrylic and ascorbic acid in gelatine initiated by copper ('MAGIC') gels (Mather *et al* 2002, Mather and Baldock 2003). US methods investigated for dose read-out are summarised in table 7, and include US CT imaging of sound speed and attenuation coefficient, backscatter attenuation estimation, backscatter B-mode, elastography (figure 8) and photoacoustics. Further work is required on batch variation and stability. This is, however, common to all gels and read-out methods (Baldock *et al* 2010). Recent work on the US read out of PAG and THPC antioxidant (PAGAT) gels shows promise (Khoei *et al* 2014), and deals with some limitations imposed by the frequency dependence of the relationship between US attenuation coefficient and dose (Crescenti *et al* 2007).

4.2. Direct US sensing of dose

Rapid and highly localised energy deposition causes a local temperature rise, and a corresponding transient increase in pressure, which propagates away from the site of absorption as

Table 7. US methods investigated for gel dosimetry. Further work is needed to reduce noise and artefact to turn each of these methods into practical dose verification tools.

Method	Gel	Property change upon irradiation, and read-out description	References
US CT	Polymer	Polymerisation changes the US speed and attenuation coefficient, which may be imaged using US transmission computed tomography methods	Mather *et al* (2002), Mather *et al* (2003), Crescenti *et al* (2007), Khoei *et al* (2014)
US backscatter attenuation estimation imaging	Polymer	Polymerisation changes the US attenuation coefficient. By adding acoustic scatterers to the gels, this may be imaged using backscatter methods for estimating attenuation	Bamber *et al* (2004)
B-mode	Polymer	Polymerisation changes the US speed and mass density, and therefore acoustic impedance. By constructing gels with distributed radiosensitive and non-radiosensitive components, acoustic impedance changes are made visible in B-mode (backscatter) images	Finlay (2005)
Elastography (SE and SWE)	Polymer	Polymerisation changes the Young's modulus. By adding acoustic scatterers to the gels, this may be imaged using SE and SWE. Under such controlled conditions, inverse reconstruction allows SE to be quantitative (figure 8), as well as SWE	Bamber *et al* (2004), Crescenti *et al* (2009a, 2009b, 2010)
Photoacoustics	Fricke xylenol	Optical absorbance of radiochromic Fricke xylenol increases with a corresponding increase in photoacoustic signal. Measurements to date have used a microphone to detect photoacoustic signals	Caldeira *et al* (2007a, 2007b)

an acoustic wave. Although this is a weak effect, the attractive proposition exists that a form of 'photoacoustography' (e.g. using x-ray photons) might be used to reconstruct the dose distribution *in vivo*. A review by Baily (1992) gives more details of the underlying physics. A desired dose sensitivity of 0.1 Gy in a single pulse of radiation requires (since the absorption of 1 Gy in water gives a temperature rise of about 0.225×10^{-3} K) a temperature sensitivity of 22.5 μK.

The subject seems to have begun with the observation at Brookhaven National Laboratory that acoustic signals consistent with thermal expansion are detectable from proton beams traversing a fluid medium (Sulak *et al* 1979). Bavizhev *et al* (1992) proposed that acoustic emissions from the absorption of heavy charged-particles could be used to determine their energy within an error of less than 3%. Tada *et al* (1991) used a hydrophone to measure acoustic signals generated in the Bragg peak of protons of therapeutic energy and intensity deposited

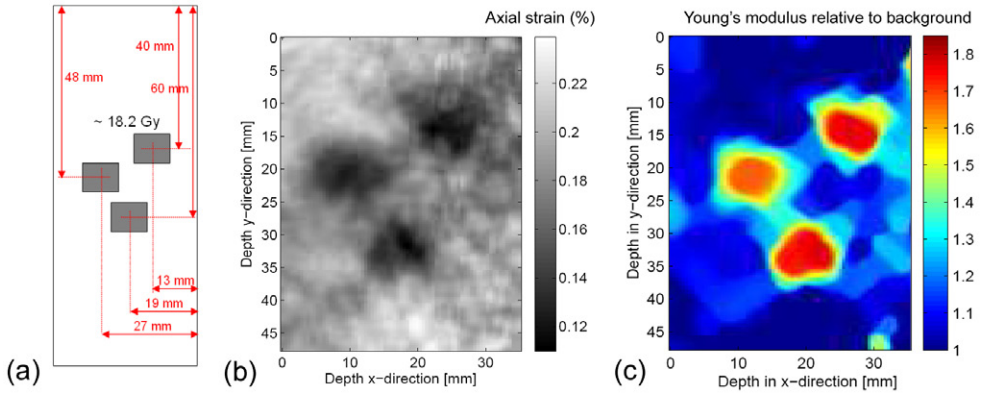

Figure 8. (a) A diagram showing the cross section of a MAGIC gel phantom and the geometry of three rod-shaped regions of square cross section each irradiated at a dose of about 18.2 Gy in a background of 0 Gy. (b) An axial strain image (derived from US measurements of displacements while axially compressing the phantom) of a central 35 mm by 48 mm area containing the three irradiated regions. (c) A relative Young's modulus map (linearly related to dose) computed by solving the plane strain inverse problem from the same displacements as used to calculate (b). Adapted with permission from Crescenti (2009).

in water and whale muscle, and proposed acoustic time-of-flight determination of the dose distribution, reporting ability to locate the distal edge of the Bragg peak to within 3 mm. This group also measured an acoustic signal from proton therapy of the liver *in vivo* (Hayakawa *et al* 1995). By combining measurements and simulation, Assmann *et al* (2015) demonstrated that a 20 MeV proton beam with 10^5 protons per (473 ns) pulse would provide adequate SNR for detection in a water phantom, corresponding to ~1.6 Gy. At higher energies within clinical scenarios SNR is reduced by increased thermal noise and scatter, spatial and temporal dose deposition broadening and increased acoustic attenuation in tissue. Simulations predict that the Bragg peak can be determined with 1 mm accuracy (Jones *et al* 2014). Assmann *et al* (2015), Hayakawa *et al* (1995) propose that higher pulse intensity and shorter (ns) pulse lengths, potentially afforded by proposed laser-based particle accelerators, may provide the SNR required to perform ionacoustical dosimetry *in vivo*. Protonacoustic tomography has also been explored for mapping the 3D proton dose distribution (Stantz *et al* 2013, Alsanea *et al* 2015).

Mascarenhas *et al* (1984) measured the photoacoustic signal from 90 kVp x-rays absorbed in a 0.2 mm lead sheet. The feasibility of US detection of the absorption of x-rays from a medical LINAC was demonstrated by Bowen *et al* (1991) and further investigated by Xiang *et al* (2013) and Hickling *et al* (2014). Substantial improvements in sensitivity appear to be needed to turn these methods into practical tools for *in vivo* RT dosimetry. However, there remains scope to explore the use of much shorter pulses of ionising radiation, which will increase the strength of the acoustic signal generated.

4.3. Speed of sound (SOS) dosimetry

SOS, reviewed by Bamber *et al* (2004), is dependent on temperature. Johnson *et al* (1975) suggested using SOS images reconstructed by time-of-flight US CT (Greenleaf *et al* 1975, Glover and Sharp 1977) to map temperature changes *in vivo* to monitor hyperthermia. The slope of SOS versus temperature is similar (and positive) for all tissues (Nasoni 1981) except fat, for which it is negative (Bamber and Hill 1979). Eventual temperature sensitivity in non-fatty

tissue of 0.2–0.5 K was predicted. US CT requires US transmission through an entire organ, and is thus applicable only to organs such as the breast. There are, however, US backscatter methods for reconstructing SOS, and recently Jaeger *et al* (2015) claimed potential resolution of about 3 (laterally) × 1 (axially) mm and SOS contrast discrimination of 0.6%. A form of backscatter US thermometry has also been evaluated for planning high intensity focused US treatments. Changes in SOS manifest in apparent tissue displacements measured using RF speckle tracking (section 2.2.1), offering potential temperature sensitivities better than 1 K (Seip *et al* 1996, Bamber 1997, Miller *et al* 2002). In practice the sensitivity of this technique is limited by variability between tissues in their strain/temperature coefficients, tissue deformation and motion (Civale *et al* 2013).

Whilst it is unlikely that the changes in SOS which result from a temperature rise in the region of tens of μK will be detectable *in vivo*, the sensitivity of SOS to local temperature changes in water after high energy deposition by ionising radiation is actively being exploited by the National Institute of Standards and Technology (NIST) (Malyarenko *et al* 2006) with the aim to replace water calorimetry as the national primary dosimetry standard; Malyarenko *et al* (2008) presented a practical 5 MHz US CT system for near real-time imaging of SOS in a water phantom which demonstrated sensitivity to sub-mK temperature changes generated by the absorption of infrared radiation. This instrument has the potential to characterise the dose profiles of therapeutic radiation beams. The authors propose improvements in sensitivity to the μK level.

5. Concluding remarks

As was indicated in figure 1, the integration of US into the RT workflow provides exciting opportunities beyond the management of inter-fraction motion, by introducing (without additional ionizing radiation exposure to normal tissues) relatively low cost, high spatial resolution, high temporal resolution imaging methods for improving: definition of the BTV for RT planning, 3D dose verification for individual patients, intra-fraction motion estimation and management, prediction and measurement of tumour response to treatment and assessment of normal tissue reaction to RT.

The methodology for US intra-fraction motion estimation has been established, providing advantages over alternative methods of high temporal sampling, non-invasiveness, ability to measure deformation and provision of continuous monitoring without additional radiation dose. Accuracy appears sufficient and, with further work, regularisation methods combined with eventual high volume rate 3D US imaging using matrix arrays and plane wave techniques look promising for providing the required reliability. System latencies seem unlikely to be a problem when using the information for real-time control of RT delivery. More clinical studies, including a range of cancer sites and the guidance of particle therapies, are required if we are to exploit the full potential of this powerful technique.

The introduction of US scanners into the treatment room and its burgeoning acceptance into the IGRT toolkit should pave the way for exciting developments in US molecular and functional imaging to be used to improve RT target definition and monitor treatment response. Conjugation of microbubbles and nanoparticles with targeting agents has opened up the possibility of acoustic and photoacoustic molecular imaging. The technological development required to translate these techniques into the clinic is underway. Work has to be done to characterise the sensitivity of these techniques to established markers of cancer that may help define a BTV and monitor treatment progression. Intrinsic US characteristics of cancer, such as abnormal vasculature or altered stiffness, can be measured with Doppler US, contrast

agents or elastography. They may not only provide the means to define and monitor the target but also could be used for daily treatment verification of the BTV. The application of US to radiation response assessment appears to be an exciting area in which new technologies such as super-resolution contrast US imaging may enable deep visualisation of microvasculature and, therefore, early measurement of response to RT *in vivo*.

Quantitative *in vivo* measures of normal tissue response to RT are needed to support (1) clinical trials evaluating new RT techniques, including anti-fibrotic, anti-angiogenic and anti-hypoxia therapies, and (2) the investigation of genetic and physiological susceptibility to radiation toxicity (Alsner *et al* 2008). Maps of the spatial distribution of toxicity severity could be compared with dose distributions to provide greater statistical power to test the relationship between dose and toxicity (Jeraj *et al* 2010). US backscatter characterisation and elastography hold promise for this, potentially providing cost effective and non-invasive *in vivo* methods to monitor the evolution of radiation toxicity in large patient populations. The introduction of spatially registered 2D and 3D US into the simulation suite and treatment room provides automated image fusion with CT and MR planning images for multi-modality target delineation. This also provides the opportunity for longitudinal studies of treatment response using functional US imaging spatially registered to the RT target volume, normal tissue and the dose distribution.

Finally, with further development, US may offer a variety of techniques suitable for wide dissemination of cost-effective 3D dosimetry. Although US dosimetry has been investigated for many years without significant impact, substantial opportunity is present for further work. It may also play a role in providing deformable 3D phantoms that can be used to develop and validate complex and dynamic RT delivery.

Acknowledgments

T O' S, J B and E H would like to gratefully acknowledge support from the Cancer research UK Programme Award C17616/A19727 and the CRUK Cancer Imaging Centre at ICR in association with MRC & Dept of Health C1060/A16464, and NHS funding to the NIHR Biomedical Research Centre at The Royal Marsden and the ICR. SvdM is funded by GROW (School for Oncology and Developmental Biology, Maastricht University).

References

Abramowitz M, Bossart E, Flook R, Wu X, Brooks R, Lachaine M, Lathuiliere F and Pollack A 2012 Noninvasive real-time prostate tracking using a transperineal ultrasound approach *Int. J. Radiat. Oncol. Biol. Phys.* **84** S133

Ackerly T, Lancaster C, Geso M and Roxby K 2011 Clinical accuracy of ExacTrac intracranial frameless stereotactic system *Med. Phys.* **38** 5040–8

Adamson J and Wu Q 2008 Prostate intrafraction motion evaluation using kV fluoroscopy during treatment delivery: a feasibility and accuracy study *Med. Phys.* **35** 1793–806

Adamson J and Wu Q 2010 Prostate intrafraction motion assessed by simultaneous kV fluoroscopy at MV delivery II: adaptive strategies *Int. J. Radiat. Oncol. Biol. Phys.* **78** 1323–30

Adriaenssens N, Belsack D, Buyl R, Ruggiero L, Breucq C, De Mey J, Lievens P and Lamote J 2012 Ultrasound elastography as an objective diagnostic measurement tool for lymphoedema of the treated breast in breast cancer patients following breast conserving surgery and radiotherapy *Radiol. Oncol.* **46** 284–95

Ahmad A, Cool D, Chew B H, Pautler S E and Peters T M 2006 3D segmentation of kidney tumors from freehand 2D ultrasound *Medical Imaging, 2006. Int. Society for Optics and Photonics* pp 61410S-61410S-11

Ahuja A T, Ho S S, Leung S F, Kew J and Metreweli C 1999 Metastatic adenopathy from nasopharyngeal carcinoma: successful response to radiation therapy assessed by color duplex sonography *AJNR Am. J. Neuroradiol.* **20** 151–6

Al-Mahrouki A A, Karshafian R, Giles A and Czarnota G J 2012 Bioeffects of ultrasound-stimulated microbubbles on endothelial cells: gene expression changes associated with radiation enhancement *in vitro Ultrasound Med. Biol.* **38** 1958–69

Alles E, Harris-Birtill D, Jaeger M and Bamber J 2013 Performance characterisation of a new clinical spectroscopic epiphotoacoustic scanner *2013 IEEE Int. Ultrasonics Symp. (IUS)* pp 1845–8

Alles E J, Jaeger M and Bamber J C 2014 Photoacoustic clutter reduction using short-lag spatial coherence weighted imaging *Ultrasonics Symp. (IUS), 2014 IEEE Int.* (IEEE) pp 41–4

Alnowami M, Alnwaimi B, Tahavori F, Copland M and Wells K 2012 A quantitative assessment of using the Kinect for Xbox360 for respiratory surface motion tracking *SPIE Medical Imaging, 2012. Int. Society for Optics and Photonics* pp 83161T-83161T1–10

Alsanea F, Moskvin V and Stantz K M 2015 Feasibility of RACT for 3D dose measurement and range verification in a water phantom *Med. Phys.* **42** 937–46

Alsner J, Andreassen C N and Overgaard J 2008 Genetic markers for prediction of normal tissue toxicity after radiotherapy *Semin. Radiat. Oncol.* **18** 126–35

Angelini E D, Homma S, Pearson G, Holmes J W and Laine A F 2005 Segmentation of real-time three-dimensional ultrasound for quantification of ventricular function: a clinical study on right and left ventricles *Ultrasound Med. Biol.* **31** 1143–58

Aoki M, Ono M, Kamikawa Y, Kozono K, Arimura H and Toyofuku F 2012 Development of real-time patient monitoring system using Microsoft Kinect *World Congress on Medical Physics and Biomedical Engineering* (*Beijing, China*, *26–31 May 2012*) (Berlin: Springer) pp 1456–9

Assmann W, Kellnberger S, Reinhardt S, Lehrack S, Edlich A, Thirolf P, Moser M, Dollinger G, Omar M and Ntziachristos V 2015 Ionoacoustic characterization of the proton Bragg peak with submillimeter accuracy *Med. Phys.* **42** 567–74

Badea A F, Szora A T, Ciuleanu E, Chioreanu I, Băciuţ G, Platon M L and Badea R 2013 ARFI quantitative elastography of the submandibular glands. Normal measurements and the diagnosis value of the method in radiation submaxillitis *Med. Ultrasonogr.* **15** 173–9

Baily N A 1992 A review of the processes by which ultrasound is generated through the interaction of ionizing radiation and irradiated materials: some possible applications *Med. Phys.* **19** 525–32

Baker K G, Robertson V J and Duck F A 2001 A review of therapeutic ultrasound: biophysical effects *Phys. Ther.* **81** 1351–8

Bakhshandeh M, Hashemi B, Mahdavi S R, Nikoofar A, Edraki H R and Kazemnejad A 2012 Evaluation of thyroid disorders during head-and-neck radiotherapy by using functional analysis and ultrasonography *Int. J. Radiat. Oncol. Biol. Phys.* **83** 198–203

Baldock C, De Deene Y, Doran S, Ibbott G, Jirasek A, Lepage M, Mcauley K, Oldham M and Schreiner L 2010 Polymer gel dosimetry *Phys. Med. Biol.* **55** R1

Balter J M, Wright J N, Newell L J, Friemel B, Dimmer S, Cheng Y, Wong J, Vertatschitsch E and Mate T P 2005 Accuracy of a wireless localization system for radiotherapy *Int. J. Radiat. Oncol. Biol. Phys.* **61** 933–7

Bamber J 1992 Speckle reduction *Clin. Diagn. Ultrasound* **28** 55–67

Bamber J C 1993 *Advances in Ultrasound Techniques and Instrumentation* ed P N T Wells (New York: Churchill Livingstone)

Bamber J C 1997 *Encyclopedia of Acoustics* ed M J Crocker (New York: Wiley)

Bamber J C 1998 Ultrasonic properties of tissues *Ultrasound in Medicine* ed F A Duck, A C Baker and H C Starritt (Bristol: Institute of Physics) pp 57–88

Bamber J C and Bush N L 1996 Freehand elasticity imaging using speckle decorrelation rate *Acoustical Imaging* (Berlin: Springer)

Bamber J and Hill C 1979 Ultrasonic attenuation and propagation speed in mammalian tissues as a function of temperature *Ultrasound Med. Biol.* **5** 149–57

Bamber J and Nassiri D 1985 Effect of gaseous inclusions on the frequency dependence of ultrasonic attenuation in liver *Ultrasound Med. Biol.* **11** 293–8

Bamber J, Bush N, Trapp J and Partridge M 2004 Backscatter readout of radiation sensitive gels *Ultrasound* **12** 230

Bamber J, Cosgrove D, Dietrich C, Fromageau J, Bojunga J, Calliada F, Cantisani V, Correas J, D'onofrio M and Drakonaki E 2013 EFSUMB guidelines and recommendations on the clinical use of ultrasound elastography. Part 1: Basic principles and technology *Ultraschall Med.* **34** 169–84

Bavizhev M D, Burlikov V L and Vorobev S A 1992 Acoustic-emission method for determination of energy of heavy charged particles *Instrum. Exp. Tech.* **34** 47–8
Bazalova-Carter M, Schlosser J, Chen J and Hristov D 2015 Monte Carlo modeling of ultrasound probes for image guided radiotherapy *Med. Phys.* **42** 5745–56
Bedford J L, Lee Y K, Wai P, South C P and Warrington A P 2009 Evaluation of the Delta4 phantom for IMRT and VMAT verification *Phys. Med. Biol.* **54** N167
Bell M A L, Byram B C, Harris E J, Evans P M and Bamber J C 2012 *In vivo* liver tracking with a high volume rate 4D ultrasound scanner and a 2D matrix array probe *Phys. Med. Biol.* **57** 1359
Bell M A L, Sen H T, Iordachita I, Kazanzides P and Wong J 2014 *In vivo* reproducibility of robotic probe placement for a novel ultrasound-guided radiation therapy system *J. Med. Imaging* **1** 025001
Berry G P, Bamber J C, Mortimer P S, Bush N L, Miller N R and Barbone P E 2008 The spatio-temporal strain response of oedematous and nonoedematous tissue to sustained compression *in vivo Ultrasound Med. Biol.* **34** 617–29
Boehm K, Salomon G, Beyer B, Schiffmann J, Simonis K, Graefen M and Budaeus L 2015 Shear wave elastography for localization of prostate cancer lesions and assessment of elasticity thresholds: implications for targeted biopsies and active surveillance protocols *J. Urol.* **193** 794–800
Bohs L N and Trahey G E 1991 A novel method for angle independent ultrasonic imaging of blood flow and tissue motion *IEEE Trans. Biomed. Eng.* **38** 280–6
Bohs L N, Friemel B H, Mcdermott B A and Trahey G E 1993 A real time system for quantifying and displaying two-dimensional velocities using ultrasound *Ultrasound Med. Biol.* **19** 751–61
Bohs L N, Friemel B H and Trahey G E 1995 Experimental velocity profiles and volumetric flow via two-dimensional speckle tracking *Ultrasound Med. Biol.* **21** 885–98
Bonnefous O and Pesque P 1986 Time domain formulation of pulse-Doppler ultrasound and blood velocity estimation by cross correlation *Ultrason. Imaging* **8** 73–85
Bowen T, Chen C, Liew S, Lutz W and Nasoni R 1991 Observation of ultrasonic emission from edges of therapeutic x-ray beams *Phys. Med. Biol.* **36** 537
Briggs K, Al Mahrouki A, Nofiele J, El-Falou A, Stanisz M, Kim H C, Kolios M C and Czarnota G J 2014 Non-invasive monitoring of ultrasound-stimulated microbubble radiation enhancement using photoacoustic imaging *Technol. Cancer Res. Treat.* **13** 435–44
Brindle K 2008 New approaches for imaging tumour responses to treatment *Nat. Rev. Cancer* **8** 94–107
Brock M, Eggert T, Palisaar R J, Roghmann F, Braun K, Löppenberg B, Sommerer F, Noldus J and Von Bodman C 2013 Multiparametric ultrasound of the prostate: adding contrast enhanced ultrasound to real-time elastography to detect histopathologically confirmed cancer *J. Urol.* **189** 93–8
Brown J M 2002 Tumor microenvironment and the response to anticancer therapy *Cancer Biol. Ther.* **1** 453–8
Brusseau E, Perrey C, Delachartre P, Vogt M, Vray D and Ermert H 2000 Axial strain imaging using a local estimation of the scaling factor from RF ultrasound signals *Ultrason. Imaging* **22** 95–107
Bryan P, Custar S, Haaga J and Balsara V 1984 Respiratory movement of the pancreas: an ultrasonic study *J. Ultrasound Med.* **3** 317–20
Burckhardt C B 1978 Speckle in ultrasound B-mode scans *IEEE Trans. Sonics Ultrason.* **25** 1–6
Bush N L, Bamber J, Barbone P E and Yarnold J 2005 Semi-quantitative freehand elastography for assessing radiation-induced breast fibrosis *Ultrasound* **13** 261
Bussels B, Goethals L, Feron M, Bielen D, Dymarkowski S, Suetens P and Haustermans K 2003 Respiration-induced movement of the upper abdominal organs: a pitfall for the three-dimensional conformal radiation treatment of pancreatic cancer *Radiother. Oncol.* **68** 69–74
Bussink J, Kaanders J H, Van Der Graaf W T and Oyen W J 2011 PET-CT for radiotherapy treatment planning and response monitoring in solid tumors *Nat. Rev. Clin. Oncol.* **8** 233–42
Butler W M, Merrick G S, Reed J L, Murray B C and Kurko B S 2013 Intrafraction displacement of prone versus supine prostate positioning monitored by real-time electromagnetic tracking *J. Appl. Clin. Med. Phys.* **14** 198–208 (PMID: 23470943)
Byram B C, Holley G, Giannantonio D and Trahey G E 2010 3-D phantom and *in vivo* cardiac speckle tracking using a matrix array and raw echo data *IEEE Trans. Ultrason. Ferroelectr. Freq. Control* **57** 839–54
Caldeira A, De Almeida A, Neto A, Baesso M, Bento A and Silva M 2007a Fricke xylenol gel characterization using a photoacustic technique *Nucl. Instrum. Methods Phys. Res.* A **582** 484–8
Caldeira A, Neto A M, Bento A, Baesso M, Silva M and De Almeida A 2007b Behavior of oxidation in the radiochromic gel dosimeter through photoacoustic technique measurements *Appl. Radiat. Isot.* **65** 605–9

Cespedes I, Ophir J and Alam S K 1997 The combined effect of signal decorrelation and random noise on the variance of time delay estimation *IEEE Trans. Ultrason. Ferroelectr. Freq. Control* **44** 220–5

Chan P, Dinniwell R, Haider M A, Cho Y-B, Jaffray D, Lockwood G, Levin W, Manchul L, Fyles A and Milosevic M 2008 Inter-and intrafractional tumor and organ movement in patients with cervical cancer undergoing radiotherapy: a cinematic-MRI point-of-interest study *Int. J. Radiat. Oncol. Biol. Phys.* **70** 1507–15

Chang Z, Liu T, Cai J, Chen Q, Wang Z and Yin F-F 2011 Evaluation of integrated respiratory gating systems on a Novalis Tx system *J. Appl. Clin. Med. Phys.* **12** 71–9 (PMID: 21844863)

Chao K C, Deasy J O, Markman J, Haynie J, Perez C A, Purdy J A and Low D A 2001 A prospective study of salivary function sparing in patients with head-and-neck cancers receiving intensity-modulated or three-dimensional radiation therapy: initial results *Int. J. Radiat. Oncol. Biol. Phys.* **49** 907–16

Chatterjee A, Alpen E L, Tobias C A, Llacer J and Alonso J 1981 High energy beams of radioactive nuclei and their biomedical applications *Int. J. Radiat. Oncol. Biol. Phys.* **7** 503–7

Chawla S, Chen Y, Katz A W, Muhs A G, Philip A, Okunieff P and Milano M T 2009 Stereotactic body radiotherapy for treatment of adrenal metastases *Int. J. Radiat. Oncol. Biol. Phys.* **75** 71–5

Chen E, Adler R, Carson P, Jenkins W and O'brien W 1995 Ultrasound tissue displacement imaging with application to breast cancer *Ultrasound Med. Biol.* **21** 1153–62

Chen J-F, Fowlkes J B, Carson P L and Rubin J M 1997 Determination of scan-plane motion using speckle decorrelation: theoretical considerations and initial test *Int. J. Imaging Syst. Technol.* **8** 38–44

Chen L, Housden R, Treece G, Gee A and Prager R 2010 *A Data Weighting Scheme for Quasistatic Ultrasound Elasticity Imaging* (Cambridge: University of Cambridge)

Cheng S C, Ying M T, Kwong D L and Wu V W 2011 Sonographic appearance of parotid glands in patients treated with intensity-modulated radiotherapy or conventional radiotherapy for nasopharyngeal carcinoma *Ultrasound Med. Biol.* **37** 220–30

Christensen-Jeffries K, Browning R J, Tang M X, Dunsby C and Eckersley R J 2014 *In vivo* acoustic super-resolution and super-resolved velocity mapping using microbubbles *IEEE Transactions on Medical Imaging* **34** 433–40

Civale J, Rivens I, Ter Haar G, Morris H, Coussios C, Friend P and Bamber J 2013 Calibration of ultrasound backscatter temperature imaging for high-intensity focused ultrasound treatment planning *Ultrasound Med. Biol.* **39** 1596–612

Coles C E, Cash C J, Treece G M, Miller F N, Hoole A C, Gee A H, Prager R W, Sinnatamby R, Britton P and Wilkinson J S 2007 High definition three-dimensional ultrasound to localise the tumour bed: a breast radiotherapy planning study *Radiother. Oncol.* **84** 233–41

Colvill E, Poulsen P R, Booth J T, O'brien R T, Ng J A and Keall P J 2014 DMLC tracking and gating can improve dose coverage for prostate VMAT *Med. Phys.* **41** 091705

Correas J-M, Tissier A-M, Khairoune A, Vassiliu V, Méjean A, Hélénon O, Memo R and Barr R G 2015 Prostate cancer: diagnostic performance of real-time shear-wave elastography *Radiology* **275** 280–9

Cosgrove D *et al* 2013 EFSUMB guidelines and recommendations on the clinical use of ultrasound elastography. Part 2: clinical applications *Ultraschall Med.* **34** 238–53

Crescenti R A 2009 Backscatter ultrasound readout of radiation-sensitive gels for radiation dosimetry *PhD Thesis* University of London

Crescenti R A, Bamber J C, Bush N L and Webb S 2009a Characterization of dose-dependent Young's modulus for a radiation-sensitive polymer gel *Phys. Med. Biol.* **54** 843

Crescenti R A, Bamber J C, Bush N L and Webb S 2009b Radiation dose imaging with ultrasound shear-wave elastography and radiation sensitive gels *2009 IEEE Int. Ultrasonics Symp. (IUS)* (IEEE) pp 495–7

Crescenti R A, Bamber J C, Oberai A A, Barbone P E, Richter J P, Rivas C, Bush N L and Webb S 2010 Quantitative ultrasonic elastography for gel dosimetry *Ultrasound Med. Biol.* **36** 268–75

Crescenti R A, Scheib S G, Schneider U and Gianolini S 2007 Introducing gel dosimetry in a clinical environment: customization of polymer gel composition and magnetic resonance imaging parameters used for 3D dose verifications in radiosurgery and intensity modulated radiotherapy *Med. Phys.* **34** 1286–97

Czarnota G, Chu W, Giles A and Kolios M 2007 Ultrasound imaging and spectrosocopy of cancer radiation therapy effects *Cancer Res.* **67** 5484

Czarnota G, Kolios M, Abraham J, Portnoy M, Ottensmeyer F, Hunt J and Sherar M 1999 Ultrasound imaging of apoptosis: high-resolution non-invasive monitoring of programmed cell death *in vitro*, *in situ* and *in vivo Br. J. Cancer* **81** 520

Czarnota G J *et al* 2012 Tumor radiation response enhancement by acoustical stimulation of the vasculature *Proc. Natl Acad. Sci. USA* **109** E2033–41
Darby S C *et al* 2013 Risk of ischemic heart disease in women after radiotherapy for breast cancer *N Engl. J. Med.* **368** 987–98
Davies S, Hill A, Holmes R, Halliwell M and Jackson P 1994 Ultrasound quantitation of respiratory organ motion in the upper abdomen *Br. J. Radiol.* **67** 1096–102
Dawson L A, Kavanagh B D, Paulino A C, Das S K, Miften M, Li X A, Pan C, Ten Haken R K and Schultheiss T E 2010 Radiation-associated kidney injury *Int. J. Radiat. Oncol. Biol. Phys.* **76** S108–15
De Los Santos J, Popple R, Agazaryan N, Bayouth J E, Bissonnette J-P, Bucci M K, Dieterich S, Dong L, Forster K M and Indelicato D 2013 Image guided radiation therapy (IGRT) technologies for radiation therapy localization and delivery *Int. J. Radiat. Oncol. Biol. Phys.* **87** 33–45
De Luca V, Benz T, Kondo S, König L, Lübke D, Rothlübbers S, Somphone O, Allaire S, Bell M L and Chung D 2015 The 2014 liver ultrasound tracking benchmark *Phys. Med. Biol.* **60** 5571
De Luca V, Tschannen M, Székely G and Tanner C 2013 A learning-based approach for fast and robust vessel tracking in long ultrasound sequences *Medical Image Computing and Computer-Assisted Intervention–MICCAI 2013* (Berlin: Springer)
Denis F, Bougnoux P, De Poncheville L, Prat M, Catroux R and Tranquart F 2002 *In vivo* quantitation of tumour vascularisation assessed by Doppler sonography in rat mammary tumours *Ultrasound Med. Biol.* **28** 431–7
Desailly Y, Couture O, Fink M and Tanter M 2013 Sono-activated ultrasound localization microscopy *Appl. Phys. Lett.* **103** 174107
Dietrich C F, Averkiou M A, Correas J M, Lassau N, Leen E and Piscaglia F 2012 An EFSUMB introduction into Dynamic Contrast-Enhanced Ultrasound (DCE-US) for quantification of tumour perfusion *Ultraschall in der Medizin* **33** 344–51
Donnelly C F, Geng L, Wojcicki W E, Fleischer A C and Hallahan D E 2001 Quantified power Doppler US of tumor blood flow correlates with microscopic quantification of tumor blood vessels *Radiology* **219** 166–70
Doran S J 2009 The history and principles of chemical dosimetry for 3-D radiation fields: gels, polymers and plastics *Appl. Radiat. Isot.* **67** 393–8
Doyley M M and Parker K J 2014 Elastography: general principles and clinical applications *Ultrasound Clin.* **9** 1–11
Doyley M M, Bamber J C, Fuechsel F and Bush N L 2001 A freehand elastographic imaging approach for clinical breast imaging: system development and performance evaluation *Ultrasound Med. Biol.* **27** 1347–57
Doyley M M, Bamber J C, Shiina T and Leach M O 1996 *Reconstruction of Elastic Modulus Distribution from Envelope Detected B-Mode Data* (Piscataway, NJ: IEEE) pp 1611–4
Duan Q, Angelini E D, Herz S L, Ingrassia C M, Costa K D, Holmes J W, Homma S and Laine A F 2009 Region-based endocardium tracking on real-time three-dimensional ultrasound *Ultrasound Med. Biol.* **35** 256–65
Eckersley R and Bamber J 2004 Methodology for imaging time-dependent phenomena *Physical Principles of Medical Ultrasonics* 2nd edn (Hoboken, NJ: Wiley) pp 303–35
Eisbruch A, Kim H M, Terrell J E, Marsh L H, Dawson L A and Ship J A 2001 Xerostomia and its predictors following parotid-sparing irradiation of head-and-neck cancer *Int. J. Radiat. Oncol. Biol. Phys.* **50** 695–704
Elie N, Kaliski A, Peronneau P, Opolon P, Roche A and Lassau N 2007 Methodology for quantifying interactions between perfusion evaluated by DCE-US and hypoxia throughout tumor growth *Ultrasound Med. Biol.* **33** 549–60
Erven K, Jurcut R, Weltens C, Giusca S, Ector J, Wildiers H, Van Den Bogaert W and Voigt J U 2011 Acute radiation effects on cardiac function detected by strain rate imaging in breast cancer patients *Int. J. Radiat. Oncol. Biol. Phys.* **79** 1444–51
Evans D H, Evans D and Mcdicken W 2000 *Doppler Ultrasound: Physics, Instrumentation, and Signal Processing* (New York: Wiley)
Fan Y, Bai J and He P 1997 Ultrasonic strain reconstruction using multi-scale cross-correlation method. Engineering in Medicine and Biology Society *Proc. of the 19th Annual Int. Conf. of the IEEE* (IEEE) pp 617–20
Feleppa E, Lizzi F, Coleman D and Yaremko M 1986 Diagnostic spectrum analysis in ophthalmology: a physical perspective *Ultrasound Med. Biol.* **12** 623–31

Feleppa E J, Porter C R, Ketterling J, Lee P, Dasgupta S, Urban S and Kalisz A 2004 Recent developments in tissue-type imaging (TTI) for planning and monitoring treatment of prostate cancer *Ultrason Imaging* **26** 163–72

Fenster A, Downey D B and Cardinal H N 2001 Three-dimensional ultrasound imaging *Phys. Med. Biol.* **46** R67–99

Ferraioli G, Filice C, Castera L, Choi B I, Sporea I, Wilson S R, Cosgrove D, Dietrich C F, Amy D and Bamber J C 2015 WFUMB guidelines and recommendations for clinical use of ultrasound elastography: part 3: liver *Ultrasound Med. Biol.* **41** 1161–79

Finlay J 2005 Ultrasonic assessment of radiation-sensitive MAGIC polymer gels *MSc Thesis* University of Exeter

Fleischer A C, Wojcicki W E, Donnelly E F, Pickens D R, Thirsk G, Thurman G B and Hellerqvist C G 1999 Quantified color Doppler sonography of tumor vascularity in an animal model *J. Ultrasound Med.* **18** 547–51

Fontanarosa D, Van Der Meer S, Bamber J, Harris E, O'Shea T and Verhaegen F 2015 Review of ultrasound image guidance in external beam radiotherapy: I. Treatment planning and inter-fraction motion management *Phys. Med. Biol.* **60** R77–114

Foroudi F, Pham D, Bressel M, Gill S and Kron T 2013 Intrafraction bladder motion in radiation therapy estimated from pretreatment and posttreatment volumetric imaging *Int. J. Radiat. Oncol. Biol. Phys.* **86** 77–82

Foroughi P, Abolmaesumi P and Hashtrudi-Zaad K 2006 Intra-subject elastic registration of 3D ultrasound images *Med. Image Anal.* **10** 713–25

Foster S G, Embree P M and O'brien W D 1990 Flow velocity profile via time-domain correlation: error analysis and computer simulation *IEEE Trans. Ultrasonics Ferroelectr. Freq. Control* **37** 164–75

Fu D and Kuduvalli G 2008 A fast, accurate, and automatic 2D–3D image registration for image-guided cranial radiosurgery *Med. Phys.* **35** 2180–94

Furukawa M K and Furukawa M 2010 Diagnosis of lymph node metastases of head and neck cancer and evaluation of effects of chemoradiotherapy using ultrasonography *Int. J. Clin. Oncol.* **15** 23–32

Gagel B *et al* 2007 pO polarography, contrast enhanced color duplex sonography (CDS), [18F] fluoromisonidazole and [18F] fluorodeoxyglucose positron emission tomography: validated methods for the evaluation of therapy-relevant tumor oxygenation or only bricks in the puzzle of tumor hypoxia? *BMC Cancer* **7** 113

Gastounioti A, Golemati S, Stoitsis J and Nikita K 2011 Comparison of Kalman-filter-based approaches for block matching in arterial wall motion analysis from B-mode ultrasound *Meas. Sci. Technol.* **22** 114008

Geiman B J, Bohs L N, Anderson M E, Breit S M and Trahey G E 2000 A novel interpolation strategy for estimating subsample speckle motion *Phys. Med. Biol.* **45** 1541

Gertsch A, Bush N, Birtill D and Bamber J 2010 Toward characterizing the size of microscopic optical absorbers using optoacoustic emission spectroscopy *BiOS, 2010. Int. Society for Optics and Photonics* pp 75641M-75641M-10

Glide-Hurst C K, Shah M M, Price R G, Liu C, Kim J, Mahan M, Fraser C, Chetty I J, Aref I and Movsas B 2015 Intrafraction variability and deformation quantification in the breast *Int. J. Radiat. Oncol. Biol. Phys.* **91** 604–11

Glover G and Sharp J 1977 Reconstruction of ultrasound propagation speed distributions in soft tissue: time-of-flight tomography *IEEE Trans. Sonics Ultrason.* **24** 229–34

Goldberg B B, Raichlen J S and Forsberg F 2001 *Ultrasound Contrast Agents: Basic Principles and Clinical Applications* (Boca Raton, FL: Informa Healthcare)

Gong R, Bruder R, Schweikard A, Schlosser J and Hristov D 2015 MO-DE-210-07: investigation of treatment interferences of a novel robotic ultrasound radiotherapy guidance system with clinical VMAT plans for liver SBRT patients *Med. Phys.* **42** 3561

Greenleaf J F 1986 *Tissue Characterization with Ultrasound* (Boca Raton, FL: CRC Press)

Greenleaf J, Johnson S, Samayoa W and Duck F 1975 Algebraic reconstruction of spatial distributions of acoustic velocities in tissue from their time-of-flight profiles *Acoustical Holography* (Berlin: Springer)

Gunarathne G P P 2013 *Breaking Through the Speed Barrier—Advancements in High-Speed Imaging* (Rijeka: InTech)

Hall T J, Zhu Y and Spalding C S 2003 *In vivo* real-time freehand palpation imaging *Ultrasound Med. Biol.* **29** 427–35

Hand J and Haar G T 1981 Heating techniques in hyperthermia *Br. J. Radiol.* **54** 443–66

Hansegård J, Orderud F and Rabben S I 2007 Real-time active shape models for segmentation of 3D cardiac ultrasound *Computer Analysis of Images and Patterns* (Berlin: Springer) pp 157–64
Hansen K L, Udesen J, Gran F, Jensen J A and Bachmann Nielsen M 2009 *In-vivo* examples of flow patterns with the fast vector velocity ultrasound method *Ultraschall Med.* **30** 471–7
Harauz G and Bronskill M 1979 Comparison of the liver's respiratory motion in the supine and upright positions: concise communication *J. Nucl. Med.* **20** 733–5
Haripotepornkul N H, Nath S K, Scanderbeg D, Saenz C and Yashar C M 2011 Evaluation of intra- and inter-fraction movement of the cervix during intensity modulated radiation therapy *Radiother. Oncol.* **98** 347–51
Harrington K J, Billingham L J, Brunner T B, Burnet N G, Chan C S, Hoskin P, Mackay R I, Maughan T S, Macdougall J and Mckenna W G 2011 Guidelines for preclinical and early phase clinical assessment of novel radiosensitisers *Br. J. Cancer* **105** 628–39
Harris E J, Miller N R, Bamber J C, Evans P M and Symonds-Tayler J R N 2007 Performance of ultrasound based measurement of 3D displacement using a curvilinear probe for organ motion tracking *Phys. Med. Biol.* **52** 5683
Harris E J, Miller N R, Bamber J C, Symonds-Tayler J R N and Evans P M 2010 Speckle tracking in a phantom and feature-based tracking in liver in the presence of respiratory motion using 4D ultrasound *Phys. Med. Biol.* **55** 3363
Harris E J, Miller N R, Bamber J C, Symonds-Tayler J R N and Evans P M 2011 The effect of object speed and direction on the performance of 3D speckle tracking using a 3D swept-volume ultrasound probe *Phys. Med. Biol.* **56** 7127
Hayakawa Y, Tada J, Arai N, Hosono K, Sato M, Wagai T, Tsuji H and Tsujii H 1995 Acoustic pulse generated in a patient during treatment by pulsed proton radiation beam *Radiat. Oncol. Investigations* **3** 42–5
Hein I and O'brien W D 1993 Current time-domain methods for assessing tissue motion by analysis from reflected ultrasound echoes—a review *IEEE Trans. Ultrason. Ferroelectr. Freq. Control* **40** 84–102
Hickling S, Hobson M and El Naqa I 2014 Feasibility of x-ray acoustic computed tomography as a tool for noninvasive volumetric *in vivo* dosimetry *Int. J. Radiat. Oncol. Biol. Phys.* **90** S843
Hill C R, Bamber J C and Ter Haar G 2004 *Physical Principles of Medical Ultrasonics* (New York: Wiley)
Hilts M, Jirasek A and Duzenli C 2005 Technical considerations for implementation of x-ray CT polymer gel dosimetry *Phys. Med. Biol.* **50** 1727
Holt J 1980 Alternative therapy for recurrent Hodgkin's disease. Radiotherapy combined with hyperthermia by electromagnetic radiation to create complete remission in 11 patients without morbidity *Br. J. Radiol.* **53** 1061–7
Hoogeman M, Prévost J-B, Nuyttens J, Pöll J, Levendag P and Heijmen B 2009 Clinical accuracy of the respiratory tumor tracking system of the cyberknife: assessment by analysis of log files *Int. J. Radiat. Oncol. Biol. Phys.* **74** 297–303
Horsman M R, Mortensen L S, Petersen J B, Busk M and Overgaard J 2012 Imaging hypoxia to improve radiotherapy outcome *Nat. Rev. Clin. Oncol.* **9** 674–87
Hossack J A, Ha J S and Sumanaweera T S 2001 Quantitative free-hand 3D ultrasound imaging based on a modified 1D transducer array *Medical Imaging Int. Society for Optics and Photonics* pp 102–12
Housden R J, Gee A H, Treece G M and Prager R W 2006 Subsample interpolation strategies for sensorless freehand 3D ultrasound *Ultrasound Med. Biol.* **32** 1897–904
Housden R J, Gee A H, Treece G M and Prager R W 2007 Sensorless reconstruction of unconstrained freehand 3D ultrasound data *Ultrasound Med. Biol.* **33** 408–19
Houston A G, Premkumar S B, Pitts D E and Babaian R J 1995 Prostate ultrasound image analysis: localization of cancer lesions to assist biopsy *Proc. of the Eighth IEEE Symp. Computer-Based Medical Systems 1995* pp 94–101
Hsu A, Miller N, Evans P, Bamber J and Webb S 2005 Feasibility of using ultrasound for real-time tracking during radiotherapy *Med. Phys.* **32** 1500–12
Huang E, Dong L, Chandra A, Kuban D A, Rosen I I, Evans A and Pollack A 2002 Intrafraction prostate motion during IMRT for prostate cancer *Int. J. Radiat. Oncol. Biol. Phys.* **53** 261–8
Huang S C, Yu C H, Huang R T, Hsu K F, Tsai Y C and Chou C Y 1996 Intratumoral blood flow in uterine myoma correlated with a lower tumor size and volume, but not correlated with cell proliferation or angiogenesis *Obstet. Gynecol.* **87** 1019–24
Huang S F, Chang R F, Moon W K, Lee Y H, Chen D R and Suri J S 2008 Analysis of tumor vascularity using three-dimensional power Doppler ultrasound images *IEEE Trans. Med. Imaging* **27** 320–30

Huang Y F, Cheng Y M, Wu Y P, Chen H H, Hsu K F, Wu Y H and Chou C Y 2013 Three-dimensional power Doppler ultrasound in cervical carcinoma: monitoring treatment response to radiotherapy *Ultrasound Obstet. Gynecol.* **42** 84–92

Hughes S, Mcclelland J, Tarte S, Lawrence D, Ahmad S, Hawkes D and Landau D 2009 Assessment of two novel ventilatory surrogates for use in the delivery of gated/tracked radiotherapy for non-small cell lung cancer *Radiother. Oncol.* **91** 336–41

Hwang S I and Lee H J 2014 The future perspectives in transrectal prostate ultrasound guided biopsy *Prostate Int.* **2** 153

Hwang M, Hariri G, Lyshchik A, Hallahan D E and Fleischer A C 2010 Correlation of quantified contrast-enhanced sonography with *in vivo* tumor response *J. Ultrasound Med.* **29** 597–607

Imanimoghaddam M, Rahrooh M, Tafakhori Z, Zahedanaraki S and Homaeieshandiz F 2012 Changes of parotid and submandibular glands caused by radiotherapy—an ultrasound evaluation *Dentomaxillofac. Radiol.* **41** 379–84

Insana M, Garra B, Rosenthal S and Hall T 1988 Quantitative ultrasonography *Med. Prog. Through Technol.* **15** 141–53

Insana M F, Hall T J and Fishback J L 1991 Identifying acoustic scattering sources in normal renal parenchyma from the anisotropy in acoustic properties *Ultrasound Med. Biol.* **17** 613–26

Insana M F, Wagner R F, Brown D G and Hall T J 1990 Describing small-scale structure in random media using pulse-echo ultrasound *J. Acoust. Soc. Am.* **87** 179–92

Jacso F, Kouznetsov A and Smith W L 2009 Development and evaluation of an ultrasound-guided tracking and gating system for hepatic radiotherapy *Med. Phys.* **36** 5633–40

Jaeger M, Bamber J C and Frenz M 2013 Clutter elimination for deep clinical optoacoustic imaging using localised vibration tagging (LOVIT) *Photoacoustics* **1** 19–29

Jaeger M, Harris-Birtill D, Gertsch A, O'flynn E and Bamber J 2012 Deformation-compensated averaging for clutter reduction in epiphotoacoustic imaging *in vivo J. Biomed. Opt.* **17** 0660071–8

Jaeger M, Held G, Peeters S, Preisser S, Grünig M and Frenz M 2015 Computed ultrasound tomography in echo mode for imaging speed of sound using pulse-echo sonography: proof of principle *Ultrasound Med. Biol.* **41** 235–50

Jaffray D A 2012 Image-guided radiotherapy: from current concept to future perspectives *Nat. Rev. Clin. Oncol.* **9** 688–99

Jamin Y *et al* 2015 Exploring the biomechanical properties of brain malignancies and their pathologic determinants *in vivo* with magnetic resonance elastography *Cancer Res.* **75** 1216–24

Jeraj R, Cao Y, Ten Haken R K, Hahn C and Marks L 2010 Imaging for assessment of radiation-induced normal tissue effects *Int. J. Radiat. Oncol. Biol. Phys.* **76** S140–4

Jiang J and Hall T J 2009 A generalized speckle tracking algorithm for ultrasonic strain imaging using dynamic programming *Ultrasound Med. Biol.* **35** 1863–79

Johnson S, Greenleaf J, Samayoa W, Duck F and Sjostrand J 1975 Reconstruction of three-dimensional velocity fields and other parameters by acoustic ray tracing *1975 Ultrasonics Symp.* (IEEE) pp 46–51

Jones K C, Witztum A, Sehgal C M and Avery S 2014 Proton beam characterization by proton-induced acoustic emission: simulation studies *Phys. Med. Biol.* **59** 6549

Jugé L, Doan B-T, Seguin J, Albuquerque M, Larrat B, Mignet N, Chabot G G, Scherman D, Paradis V and Vilgrain V 2012 Colon tumor growth and antivascular treatment in mice: complementary assessment with MR elastography and diffusion-weighted MR imaging *Radiology* **264** 436–44

Juneja P, Harris E and Bamber J 2014 SU-EJ-76: incorporation of ultrasound elastography in target volume delineation for partial breast radiotherapy planning: a comparative study *Med. Phys.* **41** 172–3

Kallel F, Bertrand M and Meunier J 1994 Speckle motion artifact under tissue rotation *IEEE Trans. Ultrason. Ferroelectr. Freq. Control* **41** 105–22

Kaneko O F and Willmann J K 2012 Ultrasound for molecular imaging and therapy in cancer *Quant. Imaging. Med. Surg.* **2** 87–97

Kass M, Witkin A and Terzopoulos D 1988 Snakes: active contour models *Int. J. Comput. Vis.* **1** 321–31

Keall P J, Todor A D, Vedam S S, Bartee C L, Siebers J V, Kini V R and Mohan R 2004 On the use of EPID-based implanted marker tracking for 4D radiotherapy *Med. Phys.* **31** 3492–9

Kerkhof E M, Van Der Put R W, Raaymakers B W, Van Der Heide U A, Jürgenliemk-Schulz I M and Lagendijk J J 2009 Intrafraction motion in patients with cervical cancer: the benefit of soft tissue registration using MRI *Radiother. Oncol.* **93** 115–21

Khoei S, Trapp J and Langton C 2014 Ultrasound attenuation computed tomography assessment of PAGAT gel dose *Phys. Med. Biol.* **59** N129

Khoo V and Joon D 2014 New developments in MRI for target volume delineation in radiotherapy *Br. J. Radiol.* **79** S2–15

Kiessling F, Fokong S, Koczera P, Lederle W and Lammers T 2012 Ultrasound microbubbles for molecular diagnosis, therapy, and theranostics *J. Nucl. Med.* **53** 345–8

Kim D W *et al* 2006 Noninvasive assessment of tumor vasculature response to radiation-mediated, vasculature-targeted therapy using quantified power Doppler sonography: implications for improvement of therapy schedules *J. Ultrasound Med.* **25** 1507–17

Kindblom J, Ekelund-Olvenmark A-M, Syren H, Iustin R, Braide K, Frank-Lissbrant I and Lennernäs B 2009 High precision transponder localization using a novel electromagnetic positioning system in patients with localized prostate cancer *Radiother. Oncol.* **90** 307–11

Kinoshita R, Shimizu S, Taguchi H, Katoh N, Fujino M, Onimaru R, Aoyama H, Katoh F, Omatsu T and Ishikawa M 2008 Three-dimensional intrafractional motion of breast during tangential breast irradiation monitored with high-sampling frequency using a real-time tumor-tracking radiotherapy system *Int. J. Radiat. Oncol. Biol. Phys.* **70** 931–4

Kirkby C, Stanescu T, Rathee S, Carlone M, Murray B and Fallone B 2008 Patient dosimetry for hybrid MRI-radiotherapy systems *Med. Phys.* **35** 1019–27

Kitamura K, Shirato H, Seppenwoolde Y, Shimizu T, Kodama Y, Endo H, Onimaru R, Oda M, Fujita K and Shimizu S 2003 Tumor location, cirrhosis, and surgical history contribute to tumor movement in the liver, as measured during stereotactic irradiation using a real-time tumor-tracking radiotherapy system *Int. J. Radiat. Oncol. Biol. Phys.* **56** 221–8

Koonce N, Chen X, Moros E, Shafirstein G, Corry P and Griffin R 2015 PET and MRI-guided focused ultrasound surgery for hypoxic-tissue ablation combined with radiotherapy in solid tumors *Int. J. Radiat. Res.* **13** 1–12

Korpanty G, Carbon J G, Grayburn P A, Fleming J B and Brekken R A 2007 Monitoring response to anticancer therapy by targeting microbubbles to tumor vasculature *Clin. Cancer Res.* **13** 323–30

Krix M, Kiessling F, Vosseler S, Farhan N, Mueller M M, Bohlen P, Fusenig N E and Delorme S 2003 Sensitive noninvasive monitoring of tumor perfusion during antiangiogenic therapy by intermittent bolus-contrast power Doppler sonography *Cancer Res.* **63** 8264–70

Krix M, Plathow C, Essig M, Herfarth K, Debus J, Kauczor H U and Delorme S 2005 Monitoring of liver metastases after stereotactic radiotherapy using low-MI contrast-enhanced ultrasound—initial results *Eur. Radiol.* **15** 677–84

Kuban D A, Dong L, Cheung R, Strom E and De Crevoisier R 2005 Ultrasound-based localization *Semin. Radiat. Oncol.* **15** 180–91

Kupelian P, Willoughby T, Mahadevan A, Djemil T, Weinstein G, Jani S, Enke C, Solberg T, Flores N and Liu D 2007 Multi-institutional clinical experience with the Calypso System in localization and continuous, real-time monitoring of the prostate gland during external radiotherapy *Int. J. Radiat. Oncol. Biol. Phys.* **67** 1088–98

Lachaine M and Falco T 2013 Intrafractional prostate motion management with the Clarity Autoscan system *Med. Phys. Int.* **1** 72–80

Landry G, Nijhuis R, Dedes G, Handrack J, Thieke C, Janssens G, De Xivry J O, Reiner M, Kamp F and Wilkens J J 2015 Investigating CT to CBCT image registration for head and neck proton therapy as a tool for daily dose recalculation *Med. Phys.* **42** 1354–66

Langeland S, D'hooge J, Torp H, Bijnens B and Suetens P 2003 Comparison of time-domain displacement estimators for two-dimensional RF tracking *Ultrasound Med. Biol.* **29** 1177–86

Langen K M and Jones D T 2001 Organ motion and its management *Int. J. Radiat. Oncol. Biol. Phys.* **50** 265–78

Langen K M, Willoughby T R, Meeks S L, Santhanam A, Cunningham A, Levine L and Kupelian P A 2008 Observations on real-time prostate gland motion using electromagnetic tracking *Int. J. Radiat. Oncol. Biol. Phys.* **71** 1084–90

Lee D, Nam W H, Lee J Y and Ra J B 2011 Non-rigid registration between 3D ultrasound and CT images of the liver based on intensity and gradient information *Phys. Med. Biol.* **56** 117

Lee J, Karshafian R, Papanicolau N, Giles A, Kolios M C and Czarnota G J 2012 Quantitative ultrasound for the monitoring of novel microbubble and ultrasound radiosensitization *Ultrasound Med. Biol.* **38** 1212–21

Lerski R, Morley P, Mills P and Watkinson G 1981 Texture analysis of ultrasonic signals—a comparison of the use of radiofrequency and demodulated A-scan data *Ultrason. Imaging* **3** 369–77

Leung S F, Zheng Y, Choi C Y, Mak S S, Chiu S K, Zee B and Mak A F 2002 Quantitative measurement of post-irradiation neck fibrosis based on the young modulus: description of a new method and clinical results *Cancer* **95** 656–62

Li J, Jamin Y, Boult J K R, Cummings C, Waterton J C, Ulloa J, Sinkus R, Bamber J C and Robinson S P 2014 Tumour biomechanical response to the vascular disrupting agent ZD6126 *in vivo* assessed by magnetic resonance elastography *Br. J. Cancer* **110** 1727–32

Li H, Kumavor P, Alqasemi U S and Zhu Q 2015 Utilizing spatial and spectral features of photoacoustic imaging for ovarian cancer detection and diagnosis *J. Biomed. Opt.* **20** 016002

Liebmann J, Cook J A, Fisher J, Teague D and Mitchell J B 1994 *In vitro* studies of Taxol as a radiation sensitizer in human tumor cells *J. Natl Cancer Inst.* **86** 441–6

Ling C C, Humm J, Larson S, Amols H, Fuks Z, Leibel S and Koutcher J A 2000 Towards multidimensional radiotherapy (MD-CRT): biological imaging and biological conformality *Int. J. Radiat. Oncol. Biol. Phys.* **47** 551–60

Linzer M and Norton S J 1982 Ultrasonic tissue characterization *Annu. Rev. Biophys. Bioeng.* **11** 303–29

Litzenberg D W, Balter J M, Hadley S W, Sandler H M, Willoughby T R, Kupelian P A and Levine L 2006 Influence of intrafraction motion on margins for prostate radiotherapy *Int. J. Radiat. Oncol. Biol. Phys.* **65** 548–53

Liu T, Zhou J, Yoshida E J, Woodhouse S A, Schiff P B, Wang T J, Lu Z F, Pile-Spellman E, Zhang P and Kutcher G J 2010 Quantitative ultrasonic evaluation of radiation-induced late tissue toxicity: pilot study of breast cancer radiotherapy *Int. J. Radiat. Oncol., Biol., Phys.* **78** 811–20

Lizzi F L, Feleppa E J, Alam S K and Deng C X 2003 Ultrasonic spectrum analysis for tissue evaluation *Pattern Recogn. Lett.* **24** 637–58

Lizzi F L, Greenebaum M, Feleppa E J, Elbaum M and Coleman D J 1983 Theoretical framework for spectrum analysis in ultrasonic tissue characterization *J. Acoust. Soc. Am.* **73** 1366–73

Mabuchi S, Sasano T, Kuroda H, Takahashi R, Nakagawa S and Kimura T 2015 Real-time tissue sonoelastography for early response monitoring in cervical cancer patients treated with definitive chemoradiotherapy: preliminary results *J. Med. Ultrason.* **42** 379–85

Malyarenko E, Heyman J, Guy S, Chen-Mayer H and Tosh R 2006 TH-E-224A-05: absorbed radiation dose measurement with a μK-resolution ultrasonic thermometer *Med. Phys.* **33** 2292

Malyarenko E V, Heyman J S, Chen-Mayer H H and Tosh R E 2008 High-resolution ultrasonic thermometer for radiation dosimetry *J Acoust. Soc. Am.* **124** 3481–90

Mancosu P, Castiglioni S, Reggiori G, Catalano M, Alongi F, Pellegrini C, Arcangeli S, Tozzi A, Lobefalo F and Fogliata A 2012 Stereotactic body radiation therapy for liver tumours using flattening filter free beam: dosimetric and technical considerations *Radiat. Oncol.* **7** 16

Maryanski M J, Schulz R J, Ibbott G S, Gatenby J C, Xie J, Horton D and Gore J C 1994 Magnetic resonance imaging of radiation dose distributions using a polymer-gel dosimeter *Phys. Med. Biol.* **39** 1437–55

Mascarenhas S, Vargas H and Cesar C 1984 A photoacoustical radiation dosimeter *Med. Phys.* **11** 73–4

Mather M L and Baldock C 2003 Ultrasound tomography imaging of radiation dose distributions in polymer gel dosimeters: preliminary study *Med. Phys.* **30** 2140–8

Mather M L, Whittaker A K and Baldock C 2002 Ultrasound evaluation of polymer gel dosimeters *Phys. Med. Biol.* **47** 1449

Matthews I, Ishikawa T and Baker S 2004 The template update problem *IEEE Trans. pattern Anal. Mach. Intell.* **26** 810–5

McBain C A, Green M, Stratford J, Davies J, Mccarthy C, Taylor B, Mchugh D, Swindell R, Khoo V and Price P 2009a Ultrasound imaging to assess inter-and intra-fraction motion during bladder radiotherapy and its potential as a verification tool *Clin. Oncol.* **21** 385–93

McBain C A, Khoo V S, Buckley D L, Sykes J S, Green M M, Cowan R A, Hutchinson C E, Moore C J and Price P M 2009b Assessment of bladder motion for clinical radiotherapy practice using cine–magnetic resonance imaging *Int. J. Radiat. Oncol. Biol. Phys.* **75** 664–71

Meijer G J, Rasch C, Remeijer P and Lebesque J V 2003 Three-dimensional analysis of delineation errors, setup errors, and organ motion during radiotherapy of bladder cancer *Int. J. Radiat. Oncol. Biol. Phys.* **55** 1277–87

Meunier J 1998 Tissue motion assessment from 3D echographic speckle tracking *Phys. Med. Biol.* **43** 1241

Meunier J and Bertrand M 1995 Echographic image mean gray level changes with tissue dynamics: a system-based model study *IEEE Trans. Biomed. Eng.* **42** 403–10

Miller N R, Bamber J C and Meaney P M 2002 Fundamental limitations of noninvasive temperature imaging by means of ultrasound echo strain estimation *Ultrasound Med. Biol.* **28** 1319–33

Miller R C, Connor W G, Heusinkveld R S and Boone M L 1977 Prospects for hyperthermia in human cancer therapy. Part I: hyperthermic effects in man and spontaneous animal tumors *Radiology* **123** 489–95

Minasian H and Bamber J 1982 A preliminary assessment of an ultrasonic Doppler method for the study of blood flow in human breast cancer *Ultrasound Med. Biol.* **8** 357–64
Montilla L G, Olafsson R, Bauer D R and Witte R S 2013 Real-time photoacoustic and ultrasound imaging: a simple solution for clinical ultrasound systems with linear arrays *Phys. Med. Biol.* **58** N1
Molloy J A and Oldham S A 2008 Benchmarking a novel ultrasound–CT fusion system for respiratory motion management in radiotherapy: assessment of spatio-temporal characteristics and comparison to 4DCT *Med. Phys.* **35** 291–300
Morsy A A and Von Ramm O T 1998 3D ultrasound tissue motion tracking using correlation search *Ultrasonic imaging* **20** 151–9
Morsy A A and Von Ramm O T 1999 FLASH correlation: a new method for 3-D ultrasound tissue motion tracking and blood velocity estimation *IEEE Trans. Ultrason. Ferroelectr. Freq. Control* **46** 728–36
Mountford R, Halliwell M and Atkinson P 1973 Ultrasonic liver scanning: automated A-scan analysis *Phys. Med. Biol.* **18** 559
Mukesh M, Barnett G, Cumming J, Wilkinson J, Moody A, Wilson C, Wishart G and Coles C 2012 Association of breast tumour bed seroma with post-operative complications and late normal tissue toxicity: results from the Cambridge Breast IMRT trial *Eur. J. Surg. Oncol. (EJSO)* **38** 918–24
Munley M T, Kagadis G C, Mcgee K P, Kirov A S, Jang S, Mutic S, Jeraj R, Xing L and Bourland J D 2013 An introduction to molecular imaging in radiation oncology: a report by the AAPM Working Group on Molecular Imaging in Radiation Oncology (WGMIR) *Med. Phys.* **40** 101501
Muren L P, Ekerold R, Kvinnsland Y, Karlsdottir À and Dahl O 2004 On the use of margins for geometrical uncertainties around the rectum in radiotherapy planning *Radiother. Oncol.* **70** 11–9
Nasoni R L 1981 Temperature corrected speed of sound for use in soft tissue imaging *Med. Phys.* **8** 513–5
Nestle U, Weber W, Hentschel M and Grosu A L 2009 Biological imaging in radiation therapy: role of positron emission tomography *Phys. Med. Biol.* **54** R1–25
Neustadter D, Barnea G, Stokar S and Corn B 2010 Analysis of dose to patient, spouse/caretaker, and staff, from an implanted trackable radioactive fiducial for use in the radiation treatment of prostate cancer *Med. Phys.* **37** 1220–4
Ng J A, Booth J T, Poulsen P R, Fledelius W, Worm E S, Eade T, Hegi F, Kneebone A, Kuncic Z and Keall P J 2012 Kilovoltage intrafraction monitoring for prostate intensity modulated arc therapy: first clinical results *Int. J. Radiat. Oncol. Biol. Phys.* **84** e655–61
Nicholas D, Nassiri D, Garbutt P and Hill C 1986 Tissue characterization from ultrasound B-scan data *Ultrasound Med. Biol.* **12** 135–43
NIH 2015a *U.S. National Institutes of Health* (Online) Available: https://clinicalTrials.gov/ct2/show/NCT02142608
NIH 2015b *U.S. National Institutes of Health* (Online) Available: https://clinicaltrials.gov/ct2/show/NCT01253213
Niizawa G *et al* 2005 Monitoring of hepatocellular carcinoma, following proton radiotherapy, with contrast-enhanced color Doppler ultrasonography *J. Gastroenterol.* **40** 283–90
Noel C, Olsen J, Green O P, Hu Y and Parikh P 2012 TU-G-217A-09: feasibility of bowel tracking using onboard cine MRI for gated radiotherapy *Med. Phys.* **39** 3928
Noel C, Parikh P J, Roy M, Kupelian P, Mahadevan A, Weinstein G, Enke C, Flores N, Beyer D and Levine L 2009 Prediction of intrafraction prostate motion: accuracy of pre-and post-treatment imaging and intermittent imaging *Int. J. Radiat. Oncol. Biol. Phys.* **73** 692–8
Noll M, Puhl J and Wesarg S 2014 Enhanced shadow detection for 3D ultrasound *Bildverarbeitung für die Medizin 2014* (Berlin: Springer)
O'Donnell M and Miller J 1981 Quantitative broadband ultrasonic backscatter: an approach to nondestructive evaluation in acoustically inhomogeneous materials *J. Appl. Phys.* **52** 1056–65
O'Shea T, Bamber J and Harris E 2015 SU-D-210-05: the accuracy of raw and B-mode image data for ultrasound speckle tracking in radiation therapy *Med. Phys.* **42** 3222
O'Shea T P, Bamber J C and Harris E J 2016 Temporal regularization of ultrasound-based liver motion estimation for image-guided radiation therapy *Med. Phys.* **43** 455–64
O'Shea T P, Garcia L J, Rosser K E, Harris E J, Evans P M and Bamber J C 2014 4D ultrasound speckle tracking of intra-fraction prostate motion: a phantom-based comparison with x-ray fiducial tracking using CyberKnife *Phys. Med. Biol.* **59** 1701
Ohlerth S, Bley C R, Laluhova D, Roos M and Kaser-Hotz B 2010 Assessment of changes in vascularity and blood volume in canine sarcomas and squamous cell carcinomas during fractionated radiation therapy using quantified contrast-enhanced power Doppler ultrasonography: a preliminary study *Vet. J.* **186** 58–63

Omari E, Noid G, Ehlers C, Erickson B, Quiroz F, Cooper D, Lachaine M and Li X 2015 SU-D-210-06: feasibility for monitoring the head of the pancreas motion through a surrogate using ultrasound during radiation therapy delivery *Med. Phys.* **42** 3223

Osmanski B-F, Pezet S, Ricobaraza A, Lenkei Z and Tanter M 2014 Functional ultrasound imaging of intrinsic connectivity in the living rat brain with high spatiotemporal resolution *Nat. Commun.* **5** 5023

Ozhasoglu C, Saw C B, Chen H, Burton S, Komanduri K, Yue N J, Huq S M and Heron D E 2008 Synchrony–cyberknife respiratory compensation technology *Med. Dosim.* **33** 117–23

Palmowski M *et al* 2009 Molecular ultrasound imaging of early vascular response in prostate tumors irradiated with carbon ions *Neoplasia* **11** 856–63

Panandiker A S P, Beltran C, Gray J and Hua C 2013 Methods for image guided and intensity modulated radiation therapy in high-risk abdominal neuroblastoma *Pract. Radiat. Oncol.* **3** 107–14

Panandiker A S P, Sharma S, Naik M H, Wu S, Hua C, Beltran C, Krasin M J and Merchant T E 2012 Novel assessment of renal motion in children as measured via four-dimensional computed tomography *Int. J. Radiat. Oncol. Biol. Phys.* **82** 1771–6

Parker K, Doyley M and Rubens D 2011 Imaging the elastic properties of tissue: the 20 year perspective *Phys. Med. Biol.* **56** R1

Parodi K, Enghardt W and Haberer T 2002 In-beam PET measurements of $\beta+$ radioactivity induced by proton beams *Phys. Med. Biol.* **47** 21

Pathak S D, Grimm P D, Chalana V and Kim Y 1998 Pubic arch detection in transrectal ultrasound guided prostate cancer therapy *IEEE Trans. Med. Imaging* **17** 762–71

Pesavento A, Lorenz A, Siebers S and Ermert H 2000 New real-time strain imaging concepts using diagnostic ultrasound *Phys. Med. Biol.* **45** 1423

Pham D, Thompson A, Kron T, Foroudi F, Kolsky M S, Devereux T, Lim A and Siva S 2014 Stereotactic ablative body radiation therapy for primary kidney cancer: a 3-dimensional conformal technique associated with low rates of early toxicity *Int. J. Radiation Oncol. Biol. Phys.* **90** 1061–8

Pirhonen J P, Grenman S A, Bredbacka A B, Bahado-Singh R O and Salmi T A 1995 Effects of external radiotherapy on uterine blood flow in patients with advanced cervical carcinoma assessed by color Doppler ultrasonography *Cancer* **76** 67–71

Piscaglia F, Nolsøe C, Dietrich C A, Cosgrove D, Gilja O, Bachmann Nielsen M, Albrecht T, Barozzi L, Bertolotto M and Catalano O 2012 The EFSUMB guidelines and recommendations on the clinical practice of contrast enhanced ultrasound (CEUS): update 2011 on non-hepatic applications *Ultraschall Med.* **33** 33

Polf J, Peterson S, Ciangaru G, Gillin M and Beddar S 2009 Prompt gamma-ray emission from biological tissues during proton irradiation: a preliminary study *Phys. Med. Biol.* **54** 731

Postema A, Idzenga T, Mischi M, Frinking P, De La Rosette J and Wijkstra H 2015a Ultrasound modalities and quantification: developments of multiparametric ultrasonography, a new modality to detect, localize and target prostatic tumors *Curr. Opin. Urol.* **25** 191–7

Postema A, Mischi M, De La Rosette J and Wijkstra H 2015b Multiparametric ultrasound in the detection of prostate cancer: a systematic review *World J. Urol.* **33** 1651–9

Prabhakar R, Kumar M, Cheruliyil S, Jayakumar S, Balasubramanian S and Cramb J 2013 Volumetric modulated arc therapy for prostate cancer patients with hip prosthesis *Rep. Pract. Oncol. Radiother.* **18** 209–13

Preisser S, Bush N L, Gertsch-Grover A G, Peeters S, Bailey A E, Bamber J C, Frenz M and Jaeger M 2013 Vessel orientation-dependent sensitivity of optoacoustic imaging using a linear array transducer *J. Biomed. Opt.* **18** 026011

Preiswerk F, De Luca V, Arnold P, Celicanin Z, Petrusca L, Tanner C, Bieri O, Salomir R and Cattin P C 2014 Model-guided respiratory organ motion prediction of the liver from 2D ultrasound *Med. Image Anal.* **18** 740–51

Qin S, Caskey C F and Ferrara K W 2009 Ultrasound contrast microbubbles in imaging and therapy: physical principles and engineering *Phys. Med. Biol.* **54** R27

Raaijmakers A, Raaymakers B and Lagendijk J 2008 Magnetic-field-induced dose effects in MR-guided radiotherapy systems: dependence on the magnetic field strength *Phys. Med. Biol.* **53** 909

Rafaelsen S R, Vagn-Hansen C, Sorensen T, Lindebjerg J, Ploen J and Jakobsen A 2013 Ultrasound elastography in patients with rectal cancer treated with chemoradiation *Eur. J. Radiol.* **82** 913–7

Ramamurthy B S and Trahey G E 1991 Potential and limitations of angle-independent flow detection algorithms using radio-frequency and detected echo signals *Ultrason. Imaging* **13** 252–68

Rapoport N, Gao Z and Kennedy A 2007 Multifunctional nanoparticles for combining ultrasonic tumor imaging and targeted chemotherapy *J. Natl Cancer Inst.* **99** 1095–106

Ravkilde T, Keall P J, Højbjerre K, Fledelius W, Worm E and Poulsen P R 2011 Geometric accuracy of dynamic MLC tracking with an implantable wired electromagnetic transponder *Acta Oncol.* **50** 944–51

Riches S, Payne G, Desouza N, Dearnaley D, Morgan V, Morgan S and Partridge M 2014 Effect on therapeutic ratio of planning a boosted radiotherapy dose to the dominant intraprostatic tumour lesion within the prostate based on multifunctional MR parameters *Br. J. Radiol.* **87** 20130813

Rivaz H, Boctor E, Foroughi P, Zellars R, Fichtinger G and Hager G 2008 Ultrasound elastography: a dynamic programming approach *IEEE Trans. Med. Imaging* **27** 1373–7

Rivaz H, Foroughi P, Fleming I, Zellars R, Boctor E and Hager G 2009 Tracked regularized ultrasound elastography for targeting breast radiotherapy *Medical Image Computing and Computer-Assisted Intervention–MICCAI 2009* (Berlin: Springer)

Rtog 2015 Available: www.rtog.org/ResearchAssociates/AdverseEventReporting/AcuteRadiationMorbidityScoringCriteria.aspx (Accessed 31/05/15)

Rubin J M, Feng M, Hadley S W, Fowlkes J B and Hamilton J D 2012 Potential use of ultrasound speckle tracking for motion management during radiotherapy preliminary report *J. Ultrasound Med.* **31** 469–81

Ruthenborg R J, Ban J-J, Wazir A, Takeda N and Kim J-W 2014 Regulation of wound healing and fibrosis by hypoxia and hypoxia-inducible factor-1 *Molecules cells* **37** 637

Rychak J J, Graba J, Cheung A M, Mystry B S, Lindner J R, Kerbel R S and Foster F S 2007 Microultrasound molecular imaging of vascular endothelial growth factor receptor 2 in a mouse model of tumor angiogenesis *Mol. Imaging* **6** 289–96

Saini R and Hoyt K 2014 Recent developments in dynamic contrast-enhanced ultrasound imaging of tumor angiogenesis *Imaging Med.* **6** 41–52

Saito K, Okura H, Watanabe N, Hayashida A, Obase K, Imai K, Maehama T, Kawamoto T, Neishi Y and Yoshida K 2009 Comprehensive evaluation of left ventricular strain using speckle tracking echocardiography in normal adults: comparison of three-dimensional and two-dimensional approaches *J. Am. Soc. Echocardiogr.* **22** 1025–30

Sartor C I 2004 Mechanisms of disease: radiosensitization by epidermal growth factor receptor inhibitors *Nat. Clin. Pract. Oncol.* **1** 80–7

Sarty G E, Liang W, Sonka M and Pierson R A 1998 Semiautomated segmentation of ovarian follicular ultrasound images using a knowledge-based algorithm *Ultrasound medicine Biol.* **24** 27–42

Sawada A, Yoda K, Kokubo M, Kunieda T, Nagata Y and Hiraoka M 2004 A technique for noninvasive respiratory gated radiation treatment system based on a real time 3D ultrasound image correlation: a phantom study *Med. Phys.* **31** 245–50

Schalk S G, Demi L, Smeenge M, Mills D M, Wallace K D, De La Rosette J J, Wijkstra H and Mischi M 2015 4-D spatiotemporal analysis of ultrasound contrast agent dispersion for prostate cancer localization: a feasibility study *IEEE Trans. Ultrason. Ferroelectr. Freq. Control* **62** 839–51

Schefter T E, Kavanagh B D, Timmerman R D, Cardenes H R, Baron A and Gaspar L E 2005 A phase I trial of stereotactic body radiation therapy (SBRT) for liver metastases *Int. J. Radiat. Oncol. Biol. Phys.* **62** 1371–8

Schifter D, Djemil T, Corn B, Mahadevan A, Lichtman R and Macklis R 2008 Target positioning accuracy of a novel technology for target localization in radiation therapy *Int. J. Radiat. Oncol. Biol. Phys.* **72** S326

Schlosser J, Salisbury K and Hristov D 2010 Telerobotic system concept for real-time soft-tissue imaging during radiotherapy beam delivery *Med. Phys.* **37** 6357–67

Schlosser J, Salisbury K and Hristov D 2011 WE-D-220-01: tissue displacement monitoring for prostate and liver IGRT using a robotically-controlled ultrasound system *Med. Phys.* **38** 3812

Schlosser J and Solek R 2015 Mechanically driven ultrasound scanning system and method *Google Patents* WO2015085257 (World Intellectual Property Organisation, Geneva, Switzerland)

Scholbach T, Scholbach J, Krombach G A, Gagel B, Maneschi P and Di Martino E 2005 New method of dynamic color doppler signal quantification in metastatic lymph nodes compared to direct polarographic measurements of tissue oxygenation *Int. J. Cancer* **114** 957–62

Schreiner L 2004 Review of Fricke gel dosimeters *J. Phys.: Conf. Ser.* **3** 003

Schwaab J, Prall M, Sarti C, Kaderka R, Bert C, Kurz C, Parodi K, Günther M and Jenne J 2014 Ultrasound tracking for intra-fractional motion compensation in radiation therapy *Phys. Med.* **30** 578–82

Scorsetti M, Mancosu P, Navarria P, Tozzi A, Castiglioni S, Clerici E, Reggiori G, Lobefalo F, Fogliata A and Cozzi L 2011 Stereotactic body radiation therapy (SBRT) for adrenal metastases *Strahlenther. Onkol.* **187** 238–44

Seip R, Vanbaren P, Cain C A and Ebbini E S 1996 Noninvasive real-time multipoint temperature control for ultrasound phased array treatments *IEEE Trans. Ultrason. Ferroelectr. Freq. Control* **43** 1063–73

Sen H T, Bell M A L, Zhang Y, Ding K, Wong J, Iordachita I and Kazanzides P 2015 System integration and preliminary *in-vivo* experiments of a robot for ultrasound guidance and monitoring during radiotherapy *2015 Int. Conf. on Advanced Robotics (ICAR)* (IEEE) pp 53–9

Shah A J, Alles E J, Box C, Eccles S A, Robinson S P and Bamber J C 2014 Non-invasive molecular profiling of cancer using photoacoustic imaging of functionalized gold nanorods *SPIE BiOS, 2014. Int. Society for Optics and Photonics* pp 89435G-89435G1–10

Shapiro M G, Goodwill P W, Neogy A, Yin M, Foster F S, Schaffer D V and Conolly S M 2014 Biogenic gas nanostructures as ultrasonic molecular reporters *Nat. Nanotechnol.* **9** 311–6

Shchory T, Harel T, Lifshitz I, Carmi-Yinon D, Kornblau G, Neustadter D and Corn B 2009 Accuracy of a radioactive tracking system in canine prostate *Int. J. Radiat. Oncol. Biol. Phys.* **75** S587

Shchory T, Schifter D, Lichtman R, Neustadter D and Corn B W 2010 Tracking accuracy of a real-time fiducial tracking system for patient positioning and monitoring in radiation therapy *Int. J. Radiat. Oncol. Biol. Phys.* **78** 1227–34

Shelton S E, Lee Y Z, Lee M, Cherin E, Foster F S, Aylward S R and Dayton P A 2015 Quantification of microvascular tortuosity during tumor evolution using acoustic angiography *Ultrasound Med. Biol.* **41** 1896–904

Shi H and Varghese T 2007 Two-dimensional multi-level strain estimation for discontinuous tissue *Phys. Med. Biol.* **52** 389

Shiina T, Doyley M and Bamber J 1996 Strain imaging using combined RF and envelope autocorrelation processing *Ultrasonics Symp., 1996. Proceedings, 1996 IEEE* (IEEE) pp 1331–6

Shiina T, Nightingale K R, Palmeri M L, Hall T J, Bamber J C, Barr R G, Castera L, Choi B I, Chou Y-H and Cosgrove D 2015 WFUMB Guidelines and recommendations for clinical use of ultrasound elastography: part 1: basic principles and terminology *Ultrasound Med. Biol.* **41** 1126–47

Shirato H, Shimizu S, Kunieda T, Kitamura K, Van Herk M, Kagei K, Nishioka T, Hashimoto S, Fujita K and Aoyama H 2000 Physical aspects of a real-time tumor-tracking system for gated radiotherapy *Int. J. Radiat. Oncol. Biol. Phys.* **48** 1187–95

Shung K K and Thieme G A 1992 *Ultrasonic Scattering in Biological Tissues* (Boca Raton, FL: CRC Press)

Stantz K, Alsanea F and Moskvin V 2013 TH-C-144-01: Best in physics (therapy)—use of radiation-induced ultrasound to image proton dosimetry *Med. Phys.* **40** 546

Stride E 2008 Physical principles of microbubbles for ultrasound imaging and therapy *Cerebrovasc. Dis.* **27** 1–13 (Suppl. 2)

Stride E and Saffari N 2003 Microbubble ultrasound contrast agents: a review *Proc. Inst. Mech. Eng.* H **217** 429–47

Sulak L, Armstrong T, Baranger H, Bregman M, Levi M, Mael D, Strait J, Bowen T, Pifer A and Polakos P 1979 Experimental studies of the acoustic signature of proton beams traversing fluid media *Nucl. Instrum. Methods* **161** 203–17

Sun J, Maeda A, Stapleton S, Chen Y, Heinmiller A, Bate D, Mcgrath T, Needles A, Theodoropoulos C and Dacosta R 2012 Monitoring radiation response in tumor vasculature using intravital photoacoustic imaging in a murine window chamber model *in vivo Cancer Res.* **72** 4338

Suramo I, Päivänsalo M and Myllylä V 1983 Cranio-caudal movements of the liver, pancreas and kidneys in respiration *Acta Radiol. Diagn.* **25** 129–31

Tachibana K 2004 Emerging technologies in therapeutic ultrasound: thermal ablation to gene delivery *Human Cell* **17** 7–15

Tada J, Hayakawa Y, Hosono K and Inada T 1991 Time resolved properties of acoustic pulses generated in water and in soft tissue by pulsed proton beam irradiation—a possibility of doses distribution monitoring in proton radiation therapy *Med. Phys.* **18** 1100–4

Tanter M and Fink M 2014 Ultrafast imaging in biomedical ultrasound *IEEE Trans. Ultrason. Ferroelectr. Freq. Control* **61** 102–19

Tavakoli V, Kemp J, Dawn B, Stoddard M and Amini A A 2010 Comparison of myocardial motion estimation methods based on simulated echocardiographic B-mode and RF data *Proc. SPIE Med. Imaging* 76260N

Taylor A and Powell M E B 2008 An assessment of interfractional uterine and cervical motion: implications for radiotherapy target volume definition in gynaecological cancer *Radiother. Oncol.* **88** 250–7

Teng J, Chen M, Gao Y, Yao Y, Chen L and Xu D 2012 Transrectal sonoelastography in the detection of prostate cancers: a meta-analysis *BJU Int.* **110** E614–20
Thomas A, Newton J, Adamovics J and Oldham M 2011 Commissioning and benchmarking a 3D dosimetry system for clinical use *Med. Phys.* **38** 4846–57
Tran W T, Iradji S, Sofroni E, Giles A, Eddy D and Czarnota G J 2012 Microbubble and ultrasound radioenhancement of bladder cancer *Br. J. Cancer* **107** 469–76
Udrescu C, Mornex F, Tanguy R and Chapet O 2013 ExacTrac snap verification: a new tool for ensuring quality control for lung stereotactic body radiation therapy *Int. J. Radiat. Oncol. Biol. Phys.* **85** e89–94
Valckx F M and Thijssen J M 1997 Characterization of echographic image texture by cooccurrence matrix parameters *Ultrasound Med. Biol.* **23** 559–71
van Elmpt W, Mcdermott L, Nijsten S, Wendling M, Lambin P and Mijnheer B 2008 A literature review of electronic portal imaging for radiotherapy dosimetry *Radiother. Oncol.* **88** 289–309
van Hove A, Savoie P-H, Maurin C, Brunelle S, Gravis G, Salem N and Walz J 2014 Comparison of image-guided targeted biopsies versus systematic randomized biopsies in the detection of prostate cancer: a systematic literature review of well-designed studies *World J. Urol.* **32** 847–58
Varghese T and Ophir J 1997 A theoretical framework for performance characterization of elastography: the strain filter *IEEE Trans. Ultrason. Ferroelectr. Freq. Control* **44** 164–72
Vergis R *et al* 2008 Intrinsic markers of tumour hypoxia and angiogenesis in localised prostate cancer and outcome of radical treatment: a retrospective analysis of two randomised radiotherapy trials and one surgical cohort study *Lancet Oncol.* **9** 342–51
Verhaegen F, Granton P and Tryggestad E 2011 Small animal radiotherapy research platforms *Phys. Med. Biol.* **56** R55
Viessmann O, Eckersley R, Christensen-Jeffries K, Tang M and Dunsby C 2013 Acoustic super-resolution with ultrasound and microbubbles *Phys. Med. Biol.* **58** 6447
Vlad R M, Brand S, Giles A, Kolios M C and Czarnota G J 2009 Quantitative ultrasound characterization of responses to radiotherapy in cancer mouse models *Clin. Cancer Res.* **15** 2067–75
Von Siebenthal M, Székely G, Gamper U, Boesiger P, Lomax A and Cattin P 2007 4D MR imaging of respiratory organ motion and its variability *Phys. Med. Biol.* **52** 1547
Waag R C 1984 A review of tissue characterization from ultrasonic scattering *IEEE Trans. Biomed. Eng.* 884–93
Wagner R F, Smith S W, Sandrik J M and Lopez H 1983 Statistics of speckle in ultrasound B-scans *IEEE Trans. Sonics Ultrason.* **30** 156–63
Walz J, Marcy M, Pianna J T, Brunelle S, Gravis G, Salem N and Bladou F 2011 Identification of the prostate cancer index lesion by real-time elastography: considerations for focal therapy of prostate cancer *World J. Urol.* **29** 589–94
Wang L V 2009 *Photoacoustic Imaging and Spectroscopy* (Boca Raton, FL: CRC Press)
Wang X, Fowlkes J B, Cannata J M, Hu C and Carson P L 2011 Photoacoustic imaging with a commercial ultrasound system and a custom probe *Ultrasound Med. Biol.* **37** 484–92
Weiss P H, Baker J M and Potchen E J 1972 Assessment of hepatic respiratory excursion *J. Nucl. Med.* **13** 758–9
Wells P S, Anderson D R, Bormanis J, Guy F, Mitchell M, Gray L, Clement C, Robinson K S and Lewandowski B 1997 Value of assessment of pretest probability of deep-vein thrombosis in clinical management *Lancet* **350** 1795–8
Wen Q, Wan S, Liu Z, Xu S, Wang H and Yang B 2014 Ultrasound contrast agents and ultrasound molecular imaging *J. Nanosci. Nanotechnol.* **14** 190–209
West C M, Cooper R A, Loncaster J A, Wilks D P and Bromley M 2001 Tumor vascularity a histological measure of angiogenesis and hypoxia *Cancer Res.* **61** 2907–10
Willoughby T R, Kupelian P A, Pouliot J, Shinohara K, Aubin M, Roach M, Skrumeda L L, Balter J M, Litzenberg D W and Hadley S W 2006 Target localization and real-time tracking using the Calypso 4D localization system in patients with localized prostate cancer *Int. J. Radiat. Oncol. Biol. Phys.* **65** 528–34
Wilson K E, Wang T Y and Willmann J K 2013 Acoustic and photoacoustic molecular imaging of cancer *J. Nucl. Med.* **54** 1851–4
Wood A K and Sehgal C M 2015 A review of low-intensity ultrasound for cancer therapy *Ultrasound Med. Biol.* **41** 905–28
Worm E S, Høyer M, Fledelius W and Poulsen P R 2013 Three-dimensional, time-resolved, intrafraction motion monitoring throughout stereotactic liver radiation therapy on a conventional linear accelerator *Int. J. Radiat. Oncol. Biol. Phys.* **86** 190–7

Wu J, Dandekar O, Nazareth D, Lei P, D'souza W and Shekhar R 2006 Effect of ultrasound probe on dose delivery during real-time ultrasound-guided tumor tracking *Engineering in Medicine and Biology Society, 2006. EMBS'06. 28th Annual Int. Conf. of the IEEE* (IEEE) pp 3799–802

Wu V W C, Ying M T C and Kwong D L W 2011 Evaluation of radiation-induced changes to parotid glands following conventional radiotherapy in patients with nasopharygneal carcinoma *Br. J. Radiol.* **84** 843–9

Xia J and Siochi R A 2012 A real-time respiratory motion monitoring system using KINECT: proof of concept *Med. Phys.* **39** 2682–5

Xiang L, Han B, Carpenter C, Pratx G, Kuang Y and Xing L 2013 X-ray acoustic computed tomography with pulsed x-ray beam from a medical linear accelerator *Med. Phys.* **40** 010701

Xu G, Meng Z-X, Lin J D, Yuan J, Carson P L, Joshi B and Wang X 2014 The functional pitch of an organ: quantification of tissue texture with photoacoustic spectrum analysis *Radiology* **271** 248–54

Xu Q and Hamilton R J 2006 A novel respiratory detection method based on automated analysis of ultrasound diaphragm video *Med. Phys.* **33** 916–21

Yang X and Fei B 2012 3D prostate segmentation of ultrasound images combining longitudinal image registration and machine learning *SPIE Medical Imaging, 2012. Int. Society for Optics and Photonics* pp 83162O1–9

Yang X, Rossi P, Jani A, Ogunleye T, Curran W and Liu T 2015 WE-EF-210-08: best in physics (imaging): 3D prostate segmentation in ultrasound images using patch-based anatomical feature *Med. Phys.* **42** 3685

Yang X, Tridandapani S, Beitler J J, David S Y, Yoshida E J, Curran W J and Liu T 2012 Ultrasound GLCM texture analysis of radiation-induced parotid-gland injury in head-and-neck cancer radiotherapy: an *in vivo* study of late toxicity *Med. Phys.* **39** 5732–9

Yarnold J and Brotons M-C V 2010 Pathogenetic mechanisms in radiation fibrosis *Radiother. Oncol.* **97** 149–61

Yarnold J, Ashton A, Bliss J, Homewood J, Harper C, Hanson J, Haviland J, Bentzen S and Owen R 2005 Fractionation sensitivity and dose response of late adverse effects in the breast after radiotherapy for early breast cancer: long-term results of a randomised trial *Radiother. Oncol.* **75** 9–17

Yeung F, Levinson S F, Fu D and Parker K J 1998 Feature-adaptive motion tracking of ultrasound image sequences using a deformable mesh *IEEE Trans. Med. Imaging* **17** 945–56

Ying M, Wu V W and Kwong D L 2007 Comparison of sonographic appearance of normal and postradiotherapy parotid glands: a preliminary study *Ultrasound Med. Biol.* **33** 1244–50

Yorke E D, Keall P and Verhaegen F 2008 Anniversary paper: role of medical physicists and the AAPM in improving geometric aspects of treatment accuracy and precision *Med. Phys.* **35** 828–39

Yoshida E J, Chen H, Torres M, Andic F, Liu H Y, Chen Z, Sun X, Curran W J and Liu T 2012 Reliability of quantitative ultrasonic assessment of normal-tissue toxicity in breast cancer radiotherapy *Int. J. Radiat. Oncol. Biol. Phys.* **82** 724–31

Zackrisson S, Van De Ven S M and Gambhir S S 2014 Light in and sound out: emerging translational strategies for photoacoustic imaging *Cancer Res.* **74** 979–1004

Zahra M A, Hollingsworth K G, Sala E, Lomas D J and Tan L T 2007 Dynamic contrast-enhanced MRI as a predictor of tumour response to radiotherapy *Lancet Oncol.* **8** 63–74

Zeidan O, Sriprisan S, Lopatiuk-Tirpak O, Kupelian P, Meeks S, Hsi W, Li Z, Palta J and Maryanski M 2010 Dosimetric evaluation of a novel polymer gel dosimeter for proton therapy *Med. Phys.* **37** 2145–52

Zhang P, Osterman K S, Liu T, Li X, Kessel J, Wu L, Schiff P and Kutcher G J 2007 How does performance of ultrasound tissue typing affect design of prostate IMRT dose-painting protocols? *Int. J. Radiat. Oncol. Biol. Phys.* **67** 362–8

Zheng Y, Leung S and Mak A 2000 Assessment of neck tissue fibrosis using an ultrasound palpation system: a feasibility study *Med. Biol. Eng. Comput.* **38** 497–502

Zhong Y, Stephans K, Qi P, Yu N, Wong J and Xia P 2013 Assessing feasibility of real-time ultrasound monitoring in stereotactic body radiotherapy of liver tumors *Technol. Cancer Res. Treat.* **12** 243–50

Zhou J, Zhang P, Osterman K S, Woodhouse S A, Schiff P B, Yoshida E J, Lu Z F, Pile-Spellman E R, Kutcher G J and Liu T 2009 Implementation and validation of an ultrasonic tissue characterization technique for quantitative assessment of normal-tissue toxicity in radiation therapy *Med. Phys.* **36** 1643–50

Ziegenhein P, Kamerling C, Heinrich H and Oelfke U 2012 SU-C-213AB-01: application of ultra-fast dose calculation in real-time interactive treatment panning *Med. Phys.* **39** 3598